J. Micropalaeontology, 44, 319–344, 2025
https://doi.org/10.5194/jm-44-319-2025


Journal of Micropalaeontology
Open Access

# Refining chitinozoan biostratigraphy through the early and late Aeronian biogeochemical events on Anticosti Island, Quebec, eastern Canada

**Fien Marie Raf Jonckheere[1,2], Carolina Klock[1], André Desrochers[3,4], Pascale Daoust[4,5], and Thijs R. A. Vandenbroucke[1]**

[1]Department of Geology, Ghent University, Ghent, 9000, Belgium
[2]Archaeology, Environmental Changes & Geo-chemistry (AMGC), Vrije Universiteit Brussel, Brussels, Belgium
[3]Department of Earth and Environmental Sciences, University of Ottawa, Ottawa, Ontario K1N 6N5, Canada
[4]Société du patrimoine mondial Anticosti, Port-Menier, QC, Canada,
[5]Earth and Planetary Sciences Department, McGill University, Montreal, QC, Canada

**Correspondence:** Fien Marie Raf Jonckheere (fien.marie.raf.jonckheere@vub.be)

Received: 15 January 2025 – Revised: 19 May 2025 – Accepted: 20 May 2025 – Published: 11 September 2025

**Abstract.** The Silurian is marked by a series of biogeochemical events that are expressed in the rock record as positive $\delta^{13}C$ excursions and that drove turnovers in marine biodiversity. Exploring these events provides a unique window into the functioning of the ancient Earth system. The anomalies in the carbon isotope record provide an excellent stratigraphic tool for global correlations in the Paleozoic. Anticosti Island has an exceptionally well-preserved stratigraphic record of the Ordovician–Silurian boundary interval, allowing for the study of the early and late Aeronian events and their impact on chitinozoan communities. This study fills a historic gap in the chitinozoan biostratigraphic record of Anticosti Island and provides a refined biostratigraphic framework for global Llandovery correlations. A total of 42 samples from the Merrimack, Gun River, Menier, and Jupiter formations near the mouth of the Jupiter River and from two cores (La Loutre and Martin La Mer) in the south-central part of the island are examined. We redefine the *Ancyrochitina ramosaspina* Local Biozone and document a total of 27 chitinozoan species. Five new species are described: *Bursachitina praedolioliformis* n. sp., *Cyathochitina triangula* n. sp., *Plectochitina triplesiensis* n. sp., *Plectochitina anulata* n. sp., and *Anthochitina admirabilis* n. sp. We formalise *B. praedolioliformis* as a smooth-walled precursor of *Eisenackitina dolioliformis*. We recognise a distinct faunal turnover at the onset of the late Aeronian event, notably represented by the appearance and radiation of diverse, highly ornamented species. This contrasts with the extinction of marine life we expected to see, based on the documented diversity loss at the onset of other Silurian events.

## 1 Introduction

During the Silurian period, marine life recovered from the oldest and second largest mass extinction in Earth's history, the Late Ordovician mass extinction (see Harper et al., 2014; Rasmussen et al., 2023). This recovery was interrupted by at least seven short-lived biogeochemical events, which happened in tandem with disruptions in the global carbon cycle, recorded as positive carbon isotope excursions and involving turnovers and extinctions in marine biodiversity (Calner, 2008; Cramer et al., 2010; Munnecke et al., 2010; Melchin et al., 2020). Nonetheless, the exact causes of these events are still a matter of debate. Emsbo (2017) demonstrated that at least one of the Silurian events, the Ireviken Event in the lowermost Wenlock, was linked to the discharge of metal-rich hydrothermal brines into the Silurian oceans, documented by SEDEX (Sedimentary Exhalative) deposits around Howard's Pass (Yukon) which ultimately triggered ocean anoxia and climate change. Vandenbroucke et al. (2015) suggested that most, if not all, of the Silurian biogeochemical events may

be ocean anoxic events (OAEs) that may not have been all that different from their more broadly studied Devonian or Mesozoic counterparts. McLaughlin et al. (2019) suggested that the coincidence of pinnacle reef development with the events and elusive negative excursions, superimposed on the otherwise positive excursions, illustrates the role of methane releases during the events. These intriguing and intricately linked hypotheses explain the continued interest in exploring new and detailed records of these events, as they provide unique windows into the inner workings of the ancient Earth system. In addition, these anomalies in the $\delta^{13}C$ record form crucial stratigraphic tools for global correlations in the Silurian and the Paleozoic as a whole (Cramer et al., 2010).

On Anticosti Island, four global positive carbon isotope excursions are recorded in the Silurian, two of which are of importance for this study. The early Aeronian event is little known, with records and research limited to Baltica and Laurentia (Kaljo et al., 2003; Braun et al., 2021). In the Baltic area, Kaljo et al. (2003) associated the early Aeronian positive $\delta^{13}C$ excursion with diamictites that are linked to a glacial event on Gondwana. On Anticosti Island, this event is represented by a twin-peaked excursion with $\delta^{13}C$ peak values of approximately $+2‰$ (Braun et al., 2021). The late Aeronian event is arguably one of the least studied Silurian events, even though its $\delta^{13}C$ peak values reach $+6‰$ on Anticosti Island, making this excursion, at least locally, of higher amplitude than the extensively studied Ireviken or the Mulde positive $\delta^{13}C$ excursions (Cramer et al., 2010). The excursion is roughly coincident with the *S. sedgwickii* graptolite zone (Cramer et al., 2010).

A large part of the relative dating of the geological units of Anticosti Island was based on brachiopod studies. The Merrimack Formation is characterised by the presence of the *Virgiana mayvillensis* Taxon Range Zone, which indicates a late Rhuddanian age (Jin and Copper, 2000). The three lower members of the Gun River Formation have a low brachiopod diversity, with no biozones established. Near the top of the Macgilvray Member, the *Kulumbella xacta* Taxon Range Zone was defined, and it has a mid-Aeronian age. The Menier Formation is characterised by the *P. palaformis* and *S. gwelani* Concurrent Zone, implying a late Aeronian age. Jin and Copper (2000) established the *Stricklandia planirostrata* Assemblage Zone in the Cybèle and Ferrum members of the Jupiter Formation, where stricklandiid brachiopods reach their highest diversity; however, this did not allow for an accurate chronostratigraphy.

The onset of other Silurian events (e.g. the Ireviken and Mulde excursions) is linked to the start of major extinctions in marine life (Munnecke et al., 2003; Cramer et al., 2012). In addition, Silurian extinctions are often announced by increased malformation in fossil plankton, which can be used to elucidate the causal mechanisms of the events at large (Munnecke et al., 2012; Delabroye et al., 2012; Vandenbroucke et al., 2015; Klock et al., 2024a; Vancoppenolle et al., 2024). Yet, changes in chitinozoan biodiversity patterns or morphologies have not been explored across the early and late Aeronian events. Research on chitinozoan biostratigraphy on Anticosti Island has primarily focused on the Ordovician–Silurian boundary, spanning the Ellis Bay and Becscie formations (Soufiane and Achab, 2000; Achab et al., 2013). Those studies also included the Merrimack and Gun River formations, where two biozones were defined (Soufiane and Achab, 2000). But for the higher Menier and Jupiter formations, only preliminary chitinozoan biostratigraphic data were acquired by Achab (1981). In addition, Klock et al. (2024b) studied the upper Jupiter and Chicotte formations, leaving a "gap" in chitinozoan biostratigraphy in the Menier Formation and the lower to mid-Jupiter Formation.

Therefore, this study aims to produce a refined chitinozoan biostratigraphy of this portion of the lithostratigraphic succession of Anticosti Island, one of the most representative Llandovery successions in the world, and to define a robust biostratigraphic framework complementing that of Soufiane and Achab (2000) and Klock et al. (2024b), by focusing on the Merrimack, Gun River, Menier, and lower Jupiter formations. Additionally, we explore whether the environmental changes that drove the biogeochemical early and late Aeronian events also affected the chitinozoan clade, i.e. whether there is a significantly elevated rate of disappearance or extinction of species and/or radiation of new species or groups in relation to the event.

Date of registration of the five new species: 6 August 2025. Registration numbers:

- *Anthochitina admirabilis*: urn:lsid:zoobank.org:act:6E66A201-6F23-4957-AE9B-3864338D009F;
- *Bursachitina praedolioliformis*: urn:lsid:zoobank.org:act:2C5974A1-4ED6-499F-9203-641BEF4814E1;
- *Cyathochitina triangula*: urn:lsid:zoobank.org:act:57DCEA96-5AFF-4362-9197-BC073B3C2544;
- *Plectochitina anulata*: urn:lsid:zoobank.org:act:AE4E9EAD-AC48-45A3-BC84-06B9EFCF5E68;
- *Plectochitina triplesiensis*: urn:lsid:zoobank.org:act:13D136CA-D396-4FEE-BEFE-A0A8622D1130.

## 2 Geological setting and sample localities

Anticosti Island is located in the Gulf of St. Lawrence in Quebec, eastern Canada (Fig. 1). The sedimentary rocks are exceptionally well preserved, making this one of the more exhaustive Ordovician–Silurian records in the world (Barnes,

1988; Long, 2007; Ghienne et al., 2014). The rock succession on Anticosti was deposited during the Late Ordovician and early Silurian, in a rapidly subsiding foreland basin (Long, 2007; Bordet et al., 2010). At that time, the Anticosti Basin was located along the eastern margin of Laurentia, at paleolatitudes of 15–20° S, and the basin deepened towards the southeast into the Iapetus Ocean (Sami and Desrochers, 1992; Long, 2007; Jin et al., 2013). The strata are mostly tectonically undisturbed and are only slightly tilted (two to three degrees) in a southward direction (Bordet et al., 2010).

The examined samples are collected from four geological formations. The upper Rhuddanian Merrimack Formation consists of fossil-rich shales, interbedded with limestones, deposited on an argillaceous mud-dominated ramp (Copper and Long, 1989; Sami and Desrochers, 1992; Copper and Jin, 2014). The Gun River Formation spans from the lower to the middle Aeronian stages and includes the Lachute, Innommée, Sandtop, and Macgilvray members (Copper et al., 2012). It is characterised by rhythmically deposited limestone interbedded with shale and grainstone (Zhang and Barnes, 2002; Copper et al., 2012). The Aeronian Menier Formation comprises the Goéland Member, which contains interbedded mudstone and limestone, and the East Point Member, consisting of encrinite and reefs (Copper and Long, 1990; Copper et al., 2012). The Aeronian Jupiter Formation is characterised by shale and interbedded micrite and calcarenite and comprises the Richardson, Cybèle, Ferrum, and Pavillon members (Copper and Long, 1990; Desrochers, 2006; Long, 2007; Clayer and Desrochers, 2014; Copper and Jin, 2015).

## 3 Methodology and material

A total of 42 samples were collected for this study, consisting of 10 samples from the La Loutre #1 drillcore (49° 35′ 18″ N, 63° 38′ 14″ W), 8 samples from the Martin La Mer core (49° 17′ 01″ N, 62° 47′ 46″ W), and 24 outcrop samples from the Jupiter coastal section, with the latter collected during field campaigns in 2017 and 2023 (Triplesia Creek: 49° 30′ 19.9″ N, 63° 37′ 52.5″ W; Cape Jupiter section 1: 49° 29′ 38.9″ N, 63° 37′ 8.4″ W; Cape Jupiter section 2: 49° 29′ 43.9″ N, 63° 37′ 12.0″ W; Cape Ottawa A: 49° 28′ 12.1″ N, 63° 36′ 43.7″ W; Cape Ottawa B: 49° 27′ 27.3″ N, 63° 37′ 4.9″ W; location of the outcrop and drill core sites in Fig. 1). For each calcareous mudstone sample, 100 to 150 g was crushed, with around 200 g crushed for limestones and 300 g for the encrinite. The palynological extraction method used at UGent to retrieve the organic fraction from rocks is based on the general principles described by Paris (1981) and Sutherland (1994). De Backer et al. (2024) described the UGent lab techniques and specifics, which are used here as well. Following the acid treatment and cleaning, the residue was sieved at 53 µm and the fraction > 53 µm was studied for chitinozoans. A ZEISS SteREO Discovery V20 microscope was used for picking a total of 300 specimens per sample, and images were made using the MIRA3 TESCAN SEM, operated with MireTCx64 software and applying accelerating voltages of 5.0 kV and a working distance of 10 mm.

## 4 Results

### 4.1 Numerical chitinozoan results

Appendix A presents the numerical overview of the raw chitinozoan data per sample. Figures 2–4 present the same data on graphical logs per individual sampled site as presence–absence data. Figure 5 provides a schematic overview of the relative abundances of the chitinozoan taxa recovered from the samples combined onto a composite log for all sites (note that the vertical axis of the composite is not to scale in order to show all samples). The Martin La Mer core data are presented in Appendix A and on the composite log in Fig. 5. From the 42 analysed samples, a total of 9005 chitinozoan specimens were SEM-imaged. The La Loutre core (C45 to C60) has the least productive samples (Fig. 2). Out of the 10 samples, only two (C45 and C46) contained the desired 300 specimens per sample. Samples C47, C48, C52, and C54 contain hardly any chitinozoans, while C49, C58, and C60 yielded intermediate numbers of specimens. Overall, the preservation of the specimens is moderate. From the Martin La Mer core (LM9 to LM200), all samples are productive, except for barren sample LM200. The overall preservation is good, except for the palynomorphs of sample LM27. The samples from the Cape Jupiter coastal section are generally very productive and contain specimens that are well preserved (Figs. 3–4). Only samples TC1 and TC2 were barren, with sample TC1 taken from a normally unfavourable lithology: encrinite (Fig. 4). The samples also contain nicely preserved acritarchs, scolecodonts, and melanosclerites.

### 4.2 Systematic description of selected taxa

Our genus definitions follow Paris et al. (1999). The specimens are further identified at the species level, except for cases of poor preservation or where only a limited number of specimens was recovered, warranting against specific identification. In the latter case, identifications are limited to the genus level or left in open nomenclature, using the guidelines of Bengtson (1988). Measurements are performed using the Fiji image processing software (Schindelin et al., 2012). Measured features are explained in Table 1, and diameter measurements are given without corrections (e.g. for flattening) applied. The average values are expressed as $\bar{x}$. All specimens and residues are stored and accessible at the Department of Geology at Ghent University, Krijgslaan 281, 9000 Ghent, Belgium, except for the holotypes, which are mounted on permanent slides and curated at the museum col-

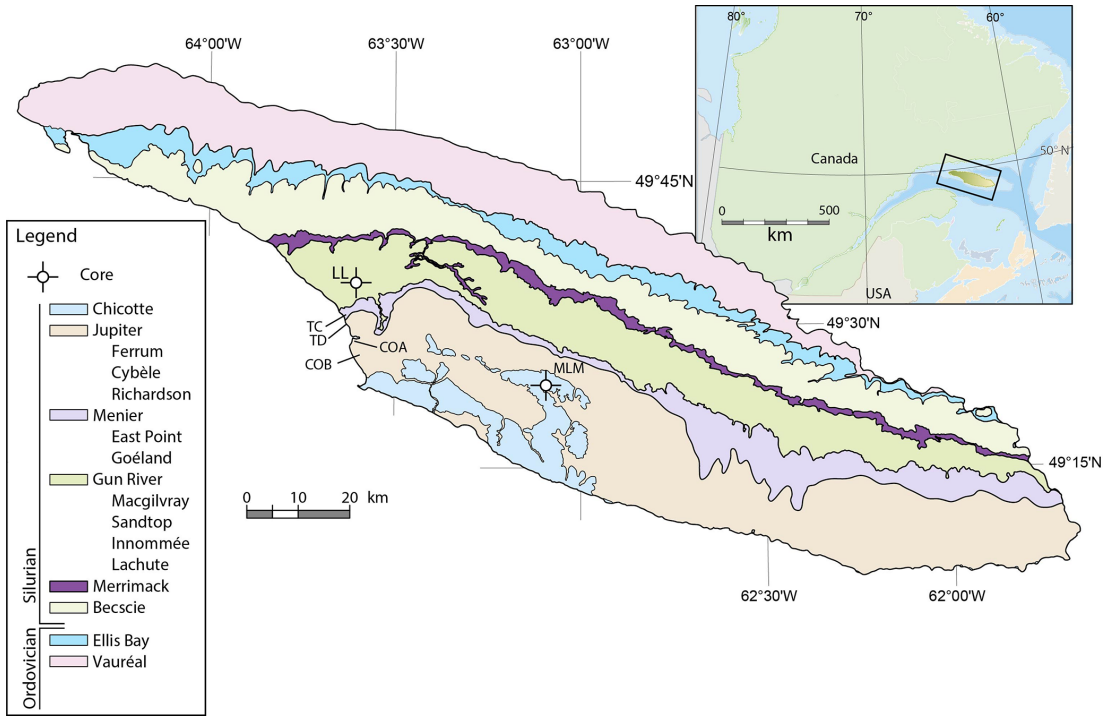


**Figure 1.** Geological map of Anticosti Island, indicating the different formations, studied members, and sample locations. Outcrop sampling localities: TC – Triplesia Creek; TD – Tidal Flats; COA – Cape Ottawa A; COB – Cape Ottawa B. Drill core localities: LL – La Loutre #1 drillcore; MLM – Martin La Mer core.

lections of the Royal Belgian Institute of Natural Sciences in Brussels (numbers IRSNB b 10053 – b 10067).

In this chapter we discuss the new taxa, taxa that diverge from published descriptions, and taxa where our observations warrant additional comments. An alphabetical list of all chitinozoan species recognised in this study is provided as Appendix B. Figures 6, 7, and 8 provide representative SEM illustrations of all recognised taxa.

Incertae sedis Group Chitinozoa Eisenack, 1931

Order Operculatifera Eisenack, 1931

Family Desmochitinidae Eisenack, 1931, emend. Paris, 1981

Subfamily Desmochitininae Paris, 1981

Genus *Calpichitina* Wilson and Hedlund, 1964

Species *Calpichitina* sp. A
Plate 1A and B

*Material*. Two specimens.

*Description*. Species with a thin-walled chamber that has a lenticular shape and bears no ornamentation. The width of the chamber ranges from 72 to 90 µm, with an average of 81 µm, and the total length of one measurable specimen is 71 µm. No flexure or neck is present, but a thin collarette widens from the aperture with a length of 2 to 8 µm.

*Dimensions*. Based upon two specimens.
Maximum width: 72 to 90 µm, $\bar{x} = 81$.
Minimum width: 71 µm.
$L/D = 0.88$.
Carina length: 2 to 8 µm, $\bar{x} = 4$ µm.
Wall thickness: 1.0 µm.

*Stratigraphic occurrence*. Occurs within the Richardson Member of the Jupiter Formation.

Genus *Bursachitina* Taugourdeau, 1966, restrict. Paris, 1981

Species *Bursachitina praedolioliformis* n. sp.
Plate 1F–I

*Derivatio nominis*. This species seems to be a precursor to the morphologically similar species *Eisenackitina dolioliformis*.

*Diagnosis*. Ovoid chamber with convex flanks and a maximum width around the middle of the chamber, a flat base with a basal scar, at times developing into a mucron, and a small neck. The wall is moderately thick and lacks ornamentation.

*Holotype*. Plate 1G.

*Holotype dimensions*. Total length = 191 µm, minimum width = 91 µm, and maximum width = 135 µm.

*Paratypes*. Plate 1F, H, and I.

*Material*. 145 specimens.

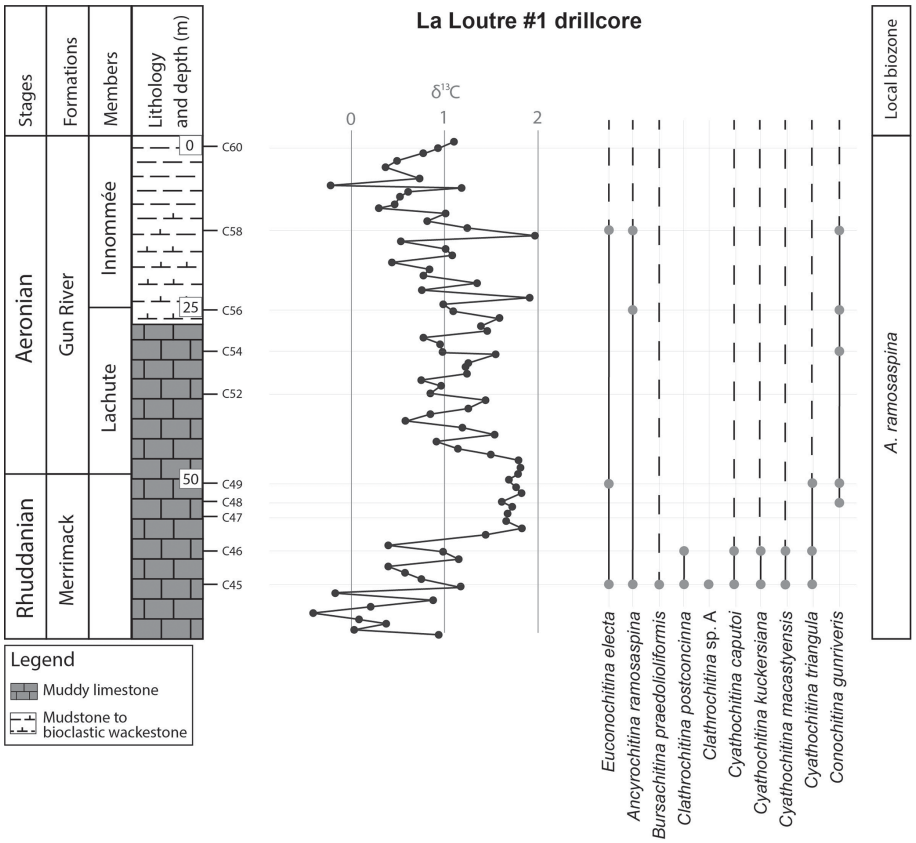


**Figure 2.** Chitinozoan ranges in the La Loutre #1 core, through the Merrimack and Gun River formations, encompassing the early Aeronian event, and the resulting local biozonation. All sample locations are indicated on the litholog. Left column shows the lithostratigraphic units, the lithology, and chitinozoan sampling levels. Middle column shows the $\delta^{13}C$ isotope data curve, measured in the same borehole (taken from and modified after Daoust, 2017).

*Type stratum*. Cybèle Member, Jupiter Formation (sample COA1).

*Description*. The total length of the vesicle is 92 to 321 µm, with an average of 188 µm. The vesicle is moderately thick walled, (2.6 µm on average). The chamber has an ovoid shape with convex flanks, a flat to slightly rounded base, and a maximum width at the middle of the chamber. The flexure is inconspicuous, and the small neck has a finely serrated lip. The base of the chamber is flat or invaginated, and the vesicle wall is glabrous. Some specimens contain a discrete basal circular scar or a prominent mucron (e.g. UK specimens).

2003 *E. dolioliformis* Umnova (1976), Vandenbroucke et al., p. 126–127, fig. 11m, n.

2013 *E. dolioliformis* Umnova (1976), Davies et al., p. 319, fig. 16d; p. 323, fig. 19.

*Dimensions*. Based upon 51 specimens.

Total length: 92 to 321 µm, $\bar{x} = 188$ µm.

Minimum width: 40 to 108 µm, $\bar{x} = 77$ µm.

Maximum width: 57 to 168 µm, $\bar{x} = 116$ µm.

$L/D = 1.95$ (with $D$ average of minimum and maximum width).

*Wall thickness*. 0.5 to 6.7 µm, $\bar{x} = 2.6$ µm.

*Stratigraphic occurrence*. Appears almost continuously through the Goéland Member of the Menier Formation and the Richardson, Cybèle, and Ferrum members of the Jupiter Formation.

*Remarks*. In terms of overall vesicle shape, this new species shows resemblance to *E. dolioliformis* and only differs from it by lacking the spines and ornamentation characteristic of *E. dolioliformis*. The specimens of the new taxon from Anticosti share the typical vesicle shape and size of *E. dolioliformis* and its thick wall. Nevertheless, we separate the unornamented species from the ornamented taxon *E. dolioliformis*. The new species is defined based on the observation of a significant number of specimens (145).

Specimens originally attributed to *E. dolioliformis* from the upper Aeronian–lower Telychian of Scotland (Vandenbroucke et al., 2003) and from the upper Aeronian of the Type Llandovery area in Wales (Davies et al., 2013), but lacking ornamentation, were originally interpreted as specimens where the ornamentation was not preserved or secondarily removed. Based on our revision, they should be reassigned to *B. praedolioliformis* n. sp.

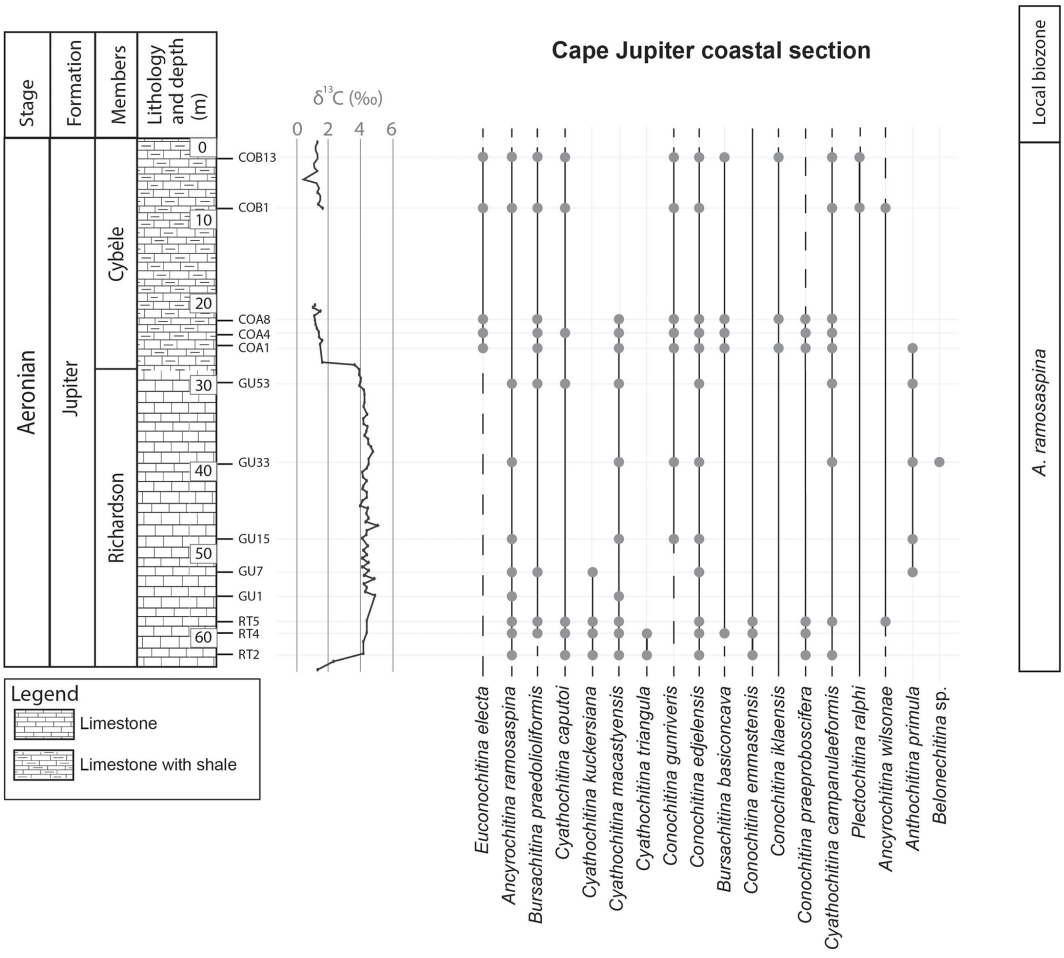


**Figure 3.** Chitinozoan ranges obtained from the Cape Jupiter coastal section, through the Richardson and Cybèle members of the Jupiter Formation. This provides chitinozoan ranges through the late Aeronian event and results in a local biozonation. The left column shows the lithostratigraphic units, the lithology, and chitinozoan sampling levels. The generalised lithostratigraphy of Anticosti Island is used as this is a composite figure. The $\delta^{13}$C isotope data curve is from Braun et al. (2021).

Order Prosomatifera Eisenack, 1972

Family Conochitinidae Eisenack, 1931 emend. Paris, 1981

Subfamily Spinachitininae Paris, 1981

Genus *Spinachitina* Schallreuter, 1963 emend. Paris, Grahn, Nestor and Lakova, 1999

Species *Spinachitina* sp. A
Plate 2B, C, and C1

*Material*. Six specimens.

*Description*. The average total length of the vesicle is 171 µm and ranges from 141 to 191 µm. The chamber is conical, with a conspicuous flexure and a wide cylindrical neck (average diameter of 51 µm). The neck flares towards the lip in a thin collarette and has single-rooted simple spines that are smaller than the spines on the chamber. The maximum width of the vesicle is at the base, and it is ornamented with randomly distributed simple spines with an average length of 2 µm. The base is flat or concave; the presence of a mucron or scar could not be established. The basal margin has a crown of 24 to 36 (an average of 29) regularly spaced processes. The processes are multirooted, simple, and thin, with an average length of eight µm.

*Dimensions*. Based upon three specimens.
Total length: 141 to 191 µm, $\bar{x} = 171$ µm.
Neck length: 61 to 81 µm, $\bar{x} = 68$ µm.
Chamber length: 77 to 122 µm, $\bar{x} = 104$ µm.
Neck diameter: 43 to 62 µm, $\bar{x} = 51$ µm.
Chamber diameter: 70 to 96 µm, $\bar{x} = 82$ µm.
$L/D = 2.09$.
Spine size: 2 to 4 µm, $\bar{x} = 2$ µm.
Process size: 5 to 10 µm, $\bar{x} = 8$ µm.
Number of processes: 24 to 36, $\bar{x} = 29$.

*Stratigraphic occurrence*. The taxon is only present in the Goéland Member of the Menier Formation.

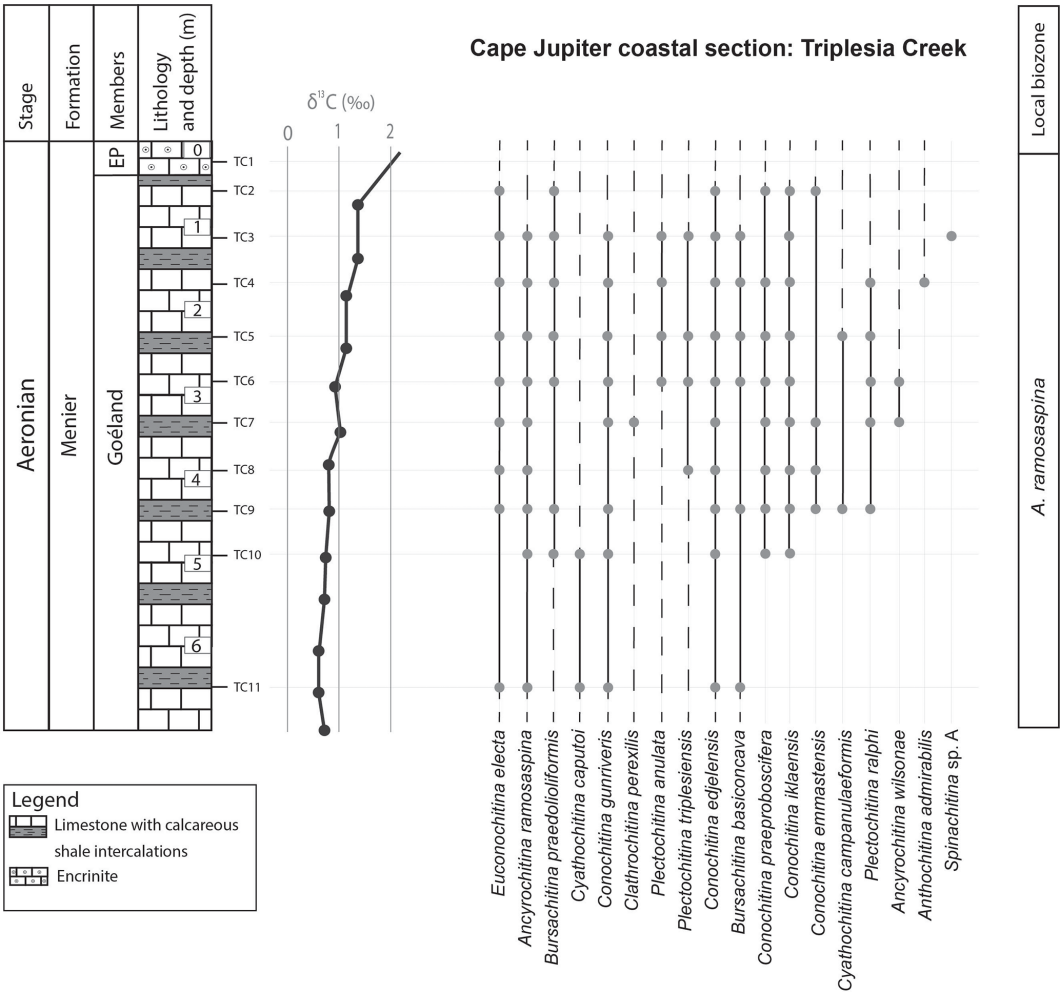


**Figure 4.** Chitinozoans from the Triplesia Creek locality, within the Menier Formation. This section records the onset of the late Aeronian event. The left column provides the lithostratigraphic units, the lithology based on field observations, and the samples taken at around 0.5 m intervals. The $\delta^{13}C$ isotope data curve is from Braun et al. (2021). EP: East Point Member.

*Remarks*. This species is different from *S. maennili* (Nestor, 1980), which has a subconical to subcylindrical shape, a narrow neck that is indistinguishable from the chamber, an ornamentation of fine grains, and a basal margin containing 8 to 20 spines that often are bi- to multirooted. *Spinachitina* sp. A, in contrast, has a more conspicuous flexure and a neck that is differentiated from the chamber, it is ornamented with actual spines rather than grains, and its processes or spines at the chamber margin are more numerous, with an average of 29 spines.

*Spinachitina* sp. A differs from *S. fragilis* (Nestor, 1980) as the latter species has no ornamentation, and a usually smoothly neck passing into the chamber is not distinguishable (Nestor, 1980), while *Spinachitina* sp. A has a distinct neck with conspicuous flexure.

*Spinachitina* sp. A differs from *S. taugourdeaui* as the latter consists of a finer, more elongated vesicle, and its spines are larger than those of *S*. sp. A.

With only six specimens of this taxon found, it would be premature to define a new species.

Family Lagenochitinidae Eisenack, 1931 emend. Paris, 1981

Subfamily Cyathochitininae Paris, 1981

Genus *Anthochitina* Eisenack, 1971

Species *Anthochitina admirabilis* n. sp.
Plate 2G, G1, and H

*Derivatio nominis*. Named after the Latin adjective *admirabilis* meaning "wonderful, astonishing", which describes the beautifully formed carina of the species.

*Diagnosis*. The thin-walled, glabrous vesicle has a chamber with straight flanks and a flat base, a conspicuous flexure, and cylindrical neck. It has a spongy and inflated carina with some large voids in it.

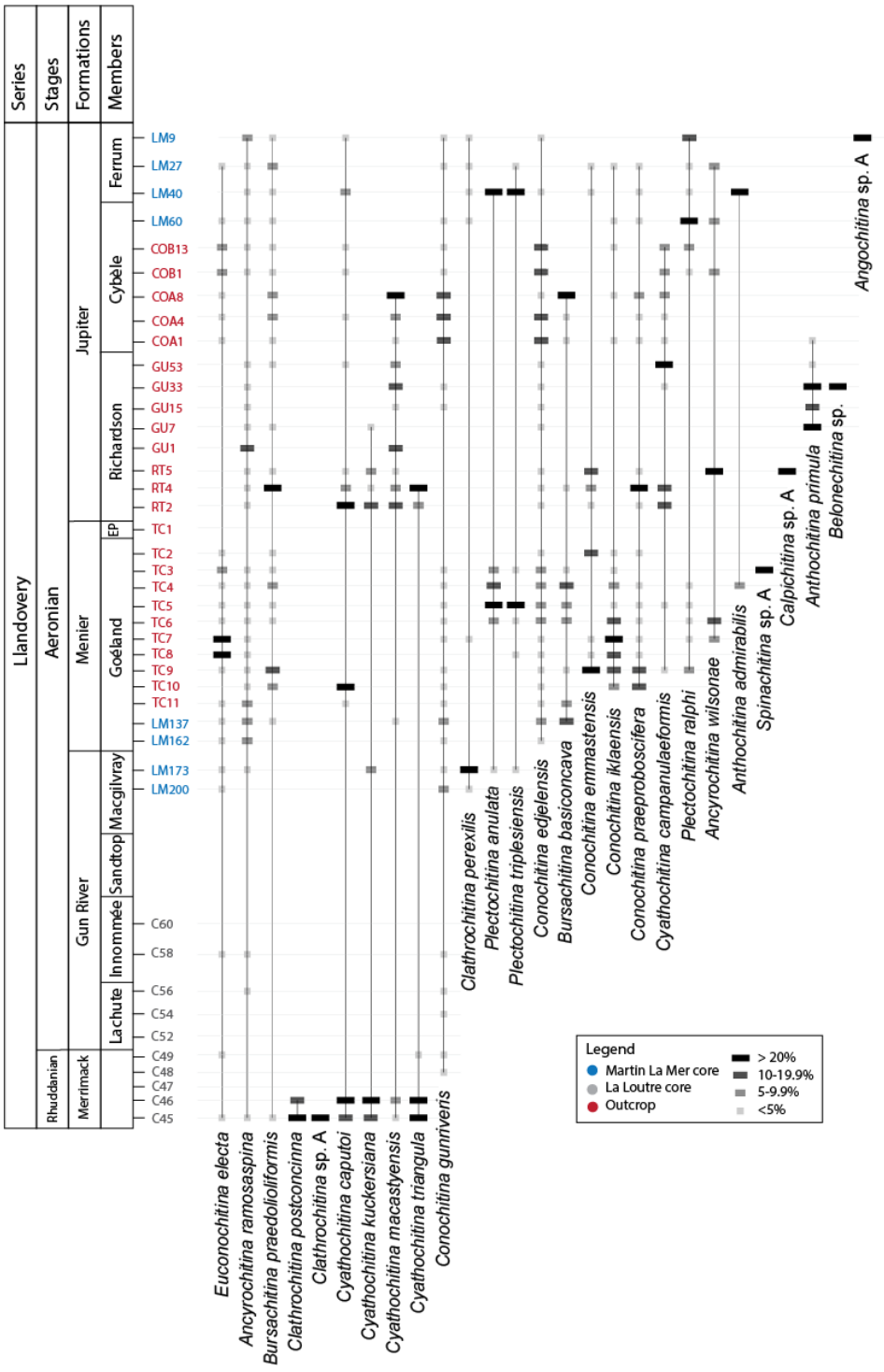


**Figure 5.** Range chart with the relative abundances of chitinozoan taxa recovered per sample in this study. Samples are approximately positioned on the vertical axis (not to scale) in the formation and member they were found in. For true vertical distribution of the samples, see Fig. 6.

**Table 1.** Description of measured features of the chitinozoans (modified after Klock et al., 2024b).

| Feature | Description |
|---|---|
| Total length | Distance from apex to aperture. |
| Neck length | Distance from aperture to flexure. |
| Chamber length | Distance from flexure to the base. |
| Neck diameter | Length of the maximum diameter of the neck. |
| Chamber diameter | Length of the base diameter if the base is the widest part of the chamber, otherwise length of the widest part of the chamber. |
| Wall thickness | Wall thickness is measured on the flanks or base of the chamber. Thin wall when $< 1.5$ µm, moderate when between 1.5 and 3.0 µm, and thick when $> 3.0$ µm. |
| Spine size | Length of the largest spine. |
| Process size | Length of the largest process. |
| Process width | Width of the widest process. |
| Carina length | Length of the carina, measured perpendicular to where the carina is attached to the chamber. |
| Carina thickness | Thickness of the carina. |
| Number of processes | Exact number of processes if the specimen is oriented in a way all processes are visible. Often the number of processes is inferred when only one side of the specimen was observable or if part of the processes has been destructed. |
| Maximum width | The largest diameter of a lenticular shape or of the chamber of specimens without a neck where the largest width typically is at the base of the chamber. |
| Minimum width | The smallest diameter of a lenticular shape or the chamber of specimens without a neck. |
| Crest height | Height of the largest crest. |

*Holotype*. Plate 2G.

*Holotype dimensions*. Neck diameter = 25.391 µm, chamber diameter = 49.408 µm, and carina length = 15.632 µm.

*Paratypes*. Plate 2H.

*Material*. 25 specimens.

*Type stratum*. Ferrum Member, Jupiter Formation (sample LM40).

*Description*. The total length of the vesicle is on average 131 µm and ranges from 97 to 159 µm. The chamber has a conical shape, with straight flanks and a flat to slightly convex base. It is thin walled, the flexure is conspicuous, and the cylindrical neck has a collarette with a finely serrated lip. The vesicle is glabrous, but it can present some discrete granules that are randomly distributed. The most distinguishing characteristic of the species is its spongy, inflated, and up to 38 µm long and 4 to 10 µm thick carina, which is continuously attached along the chamber margin. There are some large voids of up to 11 µm long in the carina (see Plate 2G1), as well as some minor perforations. When detached (e.g. Plate 2H), the carina leaves a wide, rugged, spongy scar.

*Dimensions*. Based upon 12 specimens.

Total length: 97 to 159 µm, $\bar{x} = 131$ µm.

Neck length: 42 to 84 µm, $\bar{x} = 57$ µm.

Chamber length: 55 to 96 µm, $\bar{x} = 75$ µm.

Neck diameter: 25 to 40 µm, $\bar{x} = 30$ µm.

Chamber diameter: 49 to 90 µm, $\bar{x} = 72$ µm.

$L/D = 1.82$.

Wall thickness: 0.3 to 1.3 µm, $\bar{x} = 0.9$ µm.

Length carina: 16 to 38 µm, $\bar{x} = 24$ µm.

Thickness carina: 4 to 10 µm, $\bar{x} = 7$ µm.

*Stratigraphic occurrence*. The first appearance is in the Goéland Member of the Menier Formation, and it reappears in the Ferrum Member of the Jupiter Formation.

*Remarks*. Only one specimen has a nearly fully preserved carina. Other specimens have a partially preserved or broken carina. This species shows similarities to *A. superba* (Eisenack, 1971), illustrated by Nestor (2011) in fig. 9A–D. The shape of the vesicle is similar; however, *A. superba* has a different carina. The carina of *A. superba* is flat and has an irregular edge, while the species described here have a well-delineated carina, and it is inflated rather than flat. *A. superba* is also larger, with the vesicle length ranging from 150 to 240 µm, while *A. admirabilis* n. sp. has a length of 97 to 159 µm. Despite having recovered a limited assemblage, we consider the morphology of *A. admirabilis* n. sp. to be suf-

ficiently diagnostic to warrant the formal establishment of a new species.

Genus *Cyathochitina* Eisenack, 1955 emend. Paris, Grahn, Nestor, and Lakova, 1999

Species *Cyathochitina triangula* n. sp.
Plate 2S–U

*Derivatio nominis*. Named after the triangular shape of the species.

*Diagnosis*. Conical, triangular-shaped chamber with straight flanks and wide base that narrows towards the aperture. The flexure is inconspicuous, and there is either a small neck or no neck. The base may contain a highly reduced carina or scar, although this can be absent.

*Holotype*. Plate 2S.

*Holotype dimensions*. Total length = 134 µm, minimum width = 82 µm, maximum width = 225 µm, and wall thickness = 1.2 µm.

*Paratypes*. Plate 2T and U.

*Material*. 41 specimens.

*Type stratum*. Merrimack Formation (sample C46).

*Description*. The chamber is conical, widest at the base (172 µm on average) and most narrow (53 µm on average) towards the aperture. The total length of the vesicle ranges from 107 to 196 µm, and the average is 145 µm. The flanks are straight, and the flexure inconspicuous, so no shoulder can be distinguished. The base is flat, with a highly reduced carina. This small ringlike structure on the margin extends a short distance beyond the vesicle wall in certain specimens but can also be very or even entirely reduced and/or prone to secondary removal. There is either no neck or, sometimes, a very short one (average length of 26 µm). When the neck is present, it occupies on average around 1/6 of the total length of the specimen. The chamber is glabrous and has a moderate wall thickness.

*Dimensions*. Based upon nine specimens.
Total length: 120 to 217 µm, $\bar{x} = 157$ µm.
Minimum width: 31 to 82 µm, $\bar{x} = 53$ µm.
Maximum width: 99 to 225 µm, $\bar{x} = 172$ µm.
$L/D = 1.40$ (with $D$ average of maximum and minimum width).
Wall thickness: 0.3 to 3.6 µm, $\bar{x} = 1.8$ µm.

*Stratigraphic occurrence*. Lowest occurrence in the Merrimack Formation, reappearing in the Richardson and Cybèle members of the Jupiter Formation.

*Remarks*. *C. triangula* n. sp. can be distinguished from all other *Cyathochitina* species by the strict conical, triangular chamber shape and a small neck or even no neck.

Subfamily Angochitininae Paris 1981

Genus *Angochitina* Eisenack, 1931

Species *Angochitina* sp. A sensu Klock et al., 2024b
Plate 3A

*Material*. Seven specimens.

*Dimensions*. Based upon two specimens.
Total length: 137 to 146 µm, $\bar{x} = 142$ µm.
Neck length: 73 to 80 µm, $\bar{x} = 77$ µm.
Chamber length: 63 to 68 µm, $\bar{x} = 66$ µm.
Neck diameter: 42 to 44 µm, $\bar{x} = 43$ µm.
Chamber diameter: 75 to 80 µm, $\bar{x} = 77$ µm.
$L/D = 1.84$.
Wall thickness: 0.9 to 1.1 µm, $\bar{x} = 1.0$ µm.
Spine size: 4 to 7 µm, $\bar{x} = 5$ µm.

*Stratigraphic occurrence*. Occurs in the Ferrum Member of the Jupiter Formation.

*Remarks*. This species occurs only in the top sample (LM9) of the section studied for this project. Klock et al. (2024b) sampled the top of the Ferrum Member, which is in stratigraphic continuation with the section studied herein. The specimens in both our studies belong to the same taxon.

Genus *Clathrochitina* Eisenack, 1959

Species *Clathrochitina* sp. A
Plate 3J and K

*Material*. Seven specimens.

*Description*. The vesicle length ranges from 96 to 119 µm, with an average of 107 µm, and it is thin walled. The chamber shape is conical and has convex flanks, and the flexure is conspicuous. The neck is cylindrical and widens towards the aperture, comprising a serrated lip. The mostly multirooted, small processes (average length of 19 µm) are thin and abundant and are attached to the chamber near the margin. Two to four processes can be connected at their ends and form a separate set of connected processes (Plate 3J, K). The vesicle wall contains granules that are the largest and most abundant on the chamber and three to five µm in size.

*Dimensions*. Based upon four specimens.
Total length: 96 to 119 µm, $\bar{x} = 107$ µm.
Neck length: 36 to 59 µm, $\bar{x} = 48$ µm.
Chamber length: 51 to 61 µm, $\bar{x} = 57$ µm.
Neck diameter: 32 to 37 µm, $\bar{x} = 34$ µm.
Chamber diameter: 69 to 73 µm, $\bar{x} = 81$ µm.
$L/D = 1.32$.
Wall thickness: 0.3 µm.
Spine size: 3 to 5 µm, $\bar{x} = 4$ µm.
Process size: 12 to 26 µm, $\bar{x} = 19$ µm.
Number of processes: 8 to 14, $\bar{x} = 11$.

*Stratigraphic occurrence*. Only occurs in the Merrimack Formation.

*Remarks*. Only seven specimens were found, and some of these have broken processes. So, it is not possible to exactly count the number of processes or how many are connected in one set of connected processes. Our specimens are different from *C. perexilis* and *C. postconcinna* due to their small and finer processes, the small neck, and the presence of spines on the margin.

Genus *Plectochitina* Cramer, 1964

Species *Plectochitina anulata* n. sp.
Plate 3Q, Q1, R, and S

*Derivatio nominis*. *Anulata* means "ringed" or "provided with a ring", referring to the ring structure that connects all processes.

*Diagnosis.* The smooth vesicle consists of a conical chamber with a conspicuous flexure and a cylindrical neck that flares towards the aperture. The on average 21 processes are thick, spongy, and closely spaced, and all are connected by an annular structure.

*Holotype*. Plate 3Q.

*Holotype dimensions*. Total length = 89 µm, neck length = 27 µm, chamber length = 55 µm, neck diameter = 34 µm, chamber diameter = 87 µm, process size = 26 µm, process width = 8 µm, and number of processes = 22.

*Paratypes*. Plate 3R and S.

*Material*. 24 specimens.

*Type stratum*. Goéland Member of the Menier Formation (sample TC5).

*Description*. The length of the vesicle ranges from 89 to 110 µm, with an average value of 103 µm. The shape of the chamber is conical, with straight to slightly convex flanks and a flat base. The vesicle has a conspicuous flexure and cylindrical neck that flares towards the aperture with a slightly serrated lip. The vesicle has thin walls, and it is smooth, with scarce granules over the whole vesicle. The thick processes have a spongy texture, are single-rooted, and are closely inserted next to one another. There is a single annular structure that connects all the ends of the processes, and it has the same texture as the processes. The processes range in size from 26 to 49 µm, with an average of 41 µm. The width of the processes is 7 µm on average, and a total of 18 to 26 processes are observed in the specimens, with an average of 21.

2000 *Plectochitina* sp. 2, Soufiane and Achab (2000), p. 105, plate III, fig. 6; p. 98, 107.

*Dimensions*. Based upon seven specimens.
Total length: 89 to 110 µm, $\bar{x} = 103$ µm.
Neck length: 27 to 51 µm, $\bar{x} = 39$ µm.
Chamber length: 55 to 81 µm, $\bar{x} = 63$ µm.
Neck diameter: 27 o 41 µm, $\bar{x} = 32$ µm.
Chamber diameter: 68 to 87 µm, $\bar{x} = 75$ µm.
$L/D = 1.37$.
Wall thickness: 0.5 to 0.7 µm, $\bar{x} = 0.6$ µm.
Process size: 26 to 49 µm, $\bar{x} = 41$ µm.
Process width: 3 to 11 µm, $\bar{x} = 7$ µm.
Number of processes: 18 to 26, $\bar{x} = 21$.

*Stratigraphic occurrence*. Occurs at its lowest occurrence in the Macgilvray Member of the Gun River Formation and occurs through the Goéland Member of the Menier Formation. It reappears in the Ferrum Member of the Jupiter Formation.

*Remarks*. Only a few specimens are well preserved. This species differs from *P. triplesiensis* n. sp. as the latter has fewer processes (10 on average) and the processes are connected in multiple sets of processes, while *P. anulata* has 21 processes on average and all processes are connected by one single, annular structure.

In Soufiane and Achab (2000), plate III, fig. 6, *Plectochitina* sp. 2 is shown; *Plectochitina* sp. 2 occurs in Member 4 of the Gun River Formation, which is also where *P. anulata* first appears here. It contains 14 to 19 simple processes that are connected to a concentric annular structure. The length of the specimens is 62 to 82 µm, measured on eight specimens. We consider these taxa to be conspecific, as they have similar body shapes, and their processes are similar in texture and connected by an annular ring. However, the number of well-preserved specimens in both studies is limited, and hence caution is needed. This might explain why Soufiane and Achab's specimens have 14 to 19 processes, and in this study the average is 21. The main characteristic differentiating this species is the ring connecting the processes.

This species is different from *A. admirabilis* n. sp. as *P. anulata* has many closely spaced processes connected by an annular structure, while *A. admirabilis* n. sp. does not have separate processes but a clearly defined carina. The carina has large voids in it that are fundamentally different from the spaces in between the connected processes.

*P. anulata* bears similarities to *P. filigrana* Cramer and Diez (1978), as *P. filigrana* also has multiple processes that are all connected by one ring. However, the ring in *P. filigrana* is broader and has a fine carina-like structure connecting the processes (Cramer and Diez, 1978), rather than being a delineated ring with the same texture as the processes as seen in *P. anulata*.

Species *Plectochitina triplesiensis* n. sp.
Plate 3N–P

*Derivatio nominis*. Named after Triplesia Creek, the locality where the most nicely preserved specimens are found.

*Diagnosis*. The glabrous vesicle consists of a conical chamber with straight to convex flanks, a conspicuous flexure, and a cylindrical neck with a collarette. It holds an average of 10 thick, spongy, single-rooted processes that are connected into three sets of three to five processes.

*Holotype*. Plate 3O.

*Holotype dimensions*. Neck diameter = 22 µm, chamber diameter = 62 µm, process size = 76 µm, process width = 7 µm, and number of processes = 15.

*Paratypes*. Plate 3N and P.

*Material*. 41 specimens.

*Type stratum*. Goéland Member of the Menier Formation (sample TC5).

*Description*. The vesicle length ranges from 90 to 149 µm, with an average of 119 µm. The chamber is conical, with straight to moderately convex flanks and a flat base. The flexure is conspicuous, and the cylindrical neck ends with a flaring collarette at the aperture with a finely serrated lip. The vesicle is thin walled and mostly glabrous but can contain

small granules that are distributed over the whole vesicle. The processes are wide (7 to 16 µm and on average 11 µm), are single-rooted, and have a spongy texture. They range in length from 20 to 101 µm, with an average of 56 µm. A total of 6 to 15 processes can occur, with an average of 10. Three to five processes are connected at their ends, forming one set of single-rooted anastomosing processes. Three sets of these combined processes occur per specimen.

2000 *Plectochitina* sp. 1, Soufiane and Achab (2000), p. 105, plate III, fig. 5; p. 107.

*Dimensions*. Based upon 12 specimens.
Total length: 90 to 149 µm, $\bar{x} = 119$ µm.
Neck length: 31 to 71 µm, $\bar{x} = 48$ µm.
Chamber length: 56 to 89 µm, $\bar{x} = 69$ µm.
Neck diameter: 22 to 42 µm, $\bar{x} = 33$ µm.
Chamber diameter: 62 to 99 µm, $\bar{x} = 79$ µm.
$L/D = 1.51$.
Wall thickness: 0.4 to 1.3 µm, $\bar{x} = 0.7$ µm.
Process size: 20 to 101 µm, $\bar{x} = 56$ µm.
Process width: 7 to 16 µm, $\bar{x} = 11$ µm.
Number of processes: 6 to 15, $\bar{x} = 10$.

*Stratigraphic occurrence*. Lowest occurrence in the Macgilvray Member of the Gun River Formation, through the Goéland Member of the Menier Formation. It reappears in the Ferrum Member of the Jupiter Formation.

*Remarks*. Only a few well-preserved specimens were observed. In Soufiane and Achab (2000), plate III, fig. 5, *Plectochitina* sp. 1 is shown. The basal margin of *Plectochitina* sp. 1 contains 22 to 26 small, simple anastomosing processes that form sets of four to six connected processes. It has a length of 67 to 87 µm, which is measured on only five flattened specimens. It occurs in Member 4 of the Gun River Formation, which is also where *P. triplesiensis* n. sp. first appears here. *P. triplesiensis* n. sp. and *Plectochitina* sp. 1 from Soufiane and Achab's study have a similar occurrence within the sections, as well as most characteristics such as chamber shape, and texture and organisation of the processes into multiple sets, so these taxa are likely conspecific. However, the number of well-preserved specimens in both the study of Soufiane and Achab (2000) and this study is limited. This might explain the discrepancy in the number of processes in both descriptions. The main characteristic defining the new species is that the processes are connected into multiple sets, which applies to both taxa.

## 5 Discussion

### 5.1 Chitinozoan response to biogeochemical events

The twin-peaked early Aeronian carbon isotope excursion (CIE) starts at the base of the Gun River Formation (Fig. 6). The event is preceded by a negative dip of around −1 ‰ in the $\delta^{13}C$ curve (Braun et al., 2021), which occurs in the underlying Merrimack Formation. This negative peak is not as well expressed in the $\delta^{13}C$ data of the La Loutre core (Fig. 2). The lowest sample of the La Loutre core, i.e. C45, is productive and provides a representative assemblage for that portion of the Merrimack Formation. At the onset of the event, some changes within the assemblage can be observed. Species *C. postconcinna* and *Clathrochitina* sp. A have their highest occurrence (HO) at this level, and thus they seem to disappear at the onset of the early Aeronian event. Soufiane and Achab (2000) reported that *C. postconcinna* ranges from the first to the fourth member of the Becscie Formation. Here, this species also occurs in the overlying Merrimack Formation, slightly higher than its previously published range. *B. praedolioliformis*, *C. caputoi*, *C. macastyensis*, and *C. triangula* also disappear but reappear higher up from the Menier Formation upward; i.e. they are absent in the Gun River Formation. *C. kuckersiana* reappears in the Macgilvray Member at the top of the Gun River Formation. *C. gunriveris* is reported by Soufiane and Achab (2000) to occur from the Becscie Formation to the Gun River Formation; however, in this study the species was also observed in the uppermost Merrimack Formation, at the onset of the early Aeronian event. Most of the La Loutre core samples were barren. The lack of chitinozoans might be related to the lithology and sedimentology of this part of the core, as it consists of basinal tempestites accumulated below storm wave base (Daoust, 2017). In all likelihood they represent an averse facies for the accumulation and/or preservation of chitinozoans.

The top of the Goéland Member records the onset of the late Aeronian event (Figs. 4 and 5). A clear pattern of newly appearing species is observed. Out of the 27 identified species in this study, eight have their lowest occurrence (LO) at the onset of this event, and three more occur locally, concomitant with the carbon isotope excursion (CIE). The species with their LOs immediately below the onset of the event are *C. praeproboscifera*, *C. iklaensis, C. emmastensis, C. campanulaeformis, P. ralphi, A. wilsonae*, *A. admirabilis*, and *Spinachitina* sp. A. This illustrates a radiation of species at the onset of the late Aeronian event rather than the hypothesised extinction. Similar observations suggesting radiation of species at the onset of such an event are apparent from the data of Klock et al. (2024b) for the Valgu Event, expressed higher in the stratigraphy of Anticosti Island. Around the peak of the late Aeronian CIE in the Richardson Member (Figs. 3 and 5), very short-ranging species are described (*Anthochitina primula, Angochitina* sp. A, and *Belonechitina* sp.). Additionally, *C. kuckersiana*, *C. macastyensis,* and *C. triangula* disappear in this interval. Many of the species that first occur at the onset of and during the event are highly ornamented: *A. wilsonae*, *Angochitina* sp. A, *A. primula, A. admirabilis*, *Belonechitina* sp., and *Spinachitina* sp. A. They all have well-developed processes, carinae, or spines. In addition, *C. perexilis, P. triplesiensis*, and *P. anulata* reappear briefly immediately below the event. This could indicate a reaction of chitinozoans to environmental stress, where environmental pressure drives chitinozoan morphological disparity. Possibly similar, conceptually, van de Schootbrugge


**Plate 1.** **(A–B)** *Calpichitina* sp. A (sample RT5); **(C–E)** *Bursachitina basiconcava* Soufiane and Achab (2000) (samples TC4, TC11, COA8); **(F–I)** *Bursachitina praedolioliformis* n. sp. with specimen **(G)** as the holotype and specimens **(F)**, **(H)**, and **(I)** as paratypes (samples COA4, COA1, COA1, C45); **(J–L)** *Euconochitina electa* Nestor (1980) (samples LM60, TC8, TC8); **(M–O)** *Conochitina edjelensis* Taugourdeau (1963) (samples GU33, LM137, TC4); **(P–Q)** *Conochitina emmastensis* Nestor (1982) (sample RT5); **(R–T)** *Conochitina gunriveris* Soufiane and Achab (2000) (samples COA4, C49, COA4); **(U–W)** *Conochitina iklaensis* Nestor (1980) (samples TC3, TC6, TC7); **(X–Z)** *Conochitina praeproboscifera* Nestor (1994) (samples RT4, RT4, COA8). The 25 µm scale bar applies to specimens **(A)** and **(B)**. The left-hand side 100 µm scale bar applies to specimens **(C)**–**(W)**, and the 100 µm scale bar to the right concerns specimens **(X)**–**(Z)**.

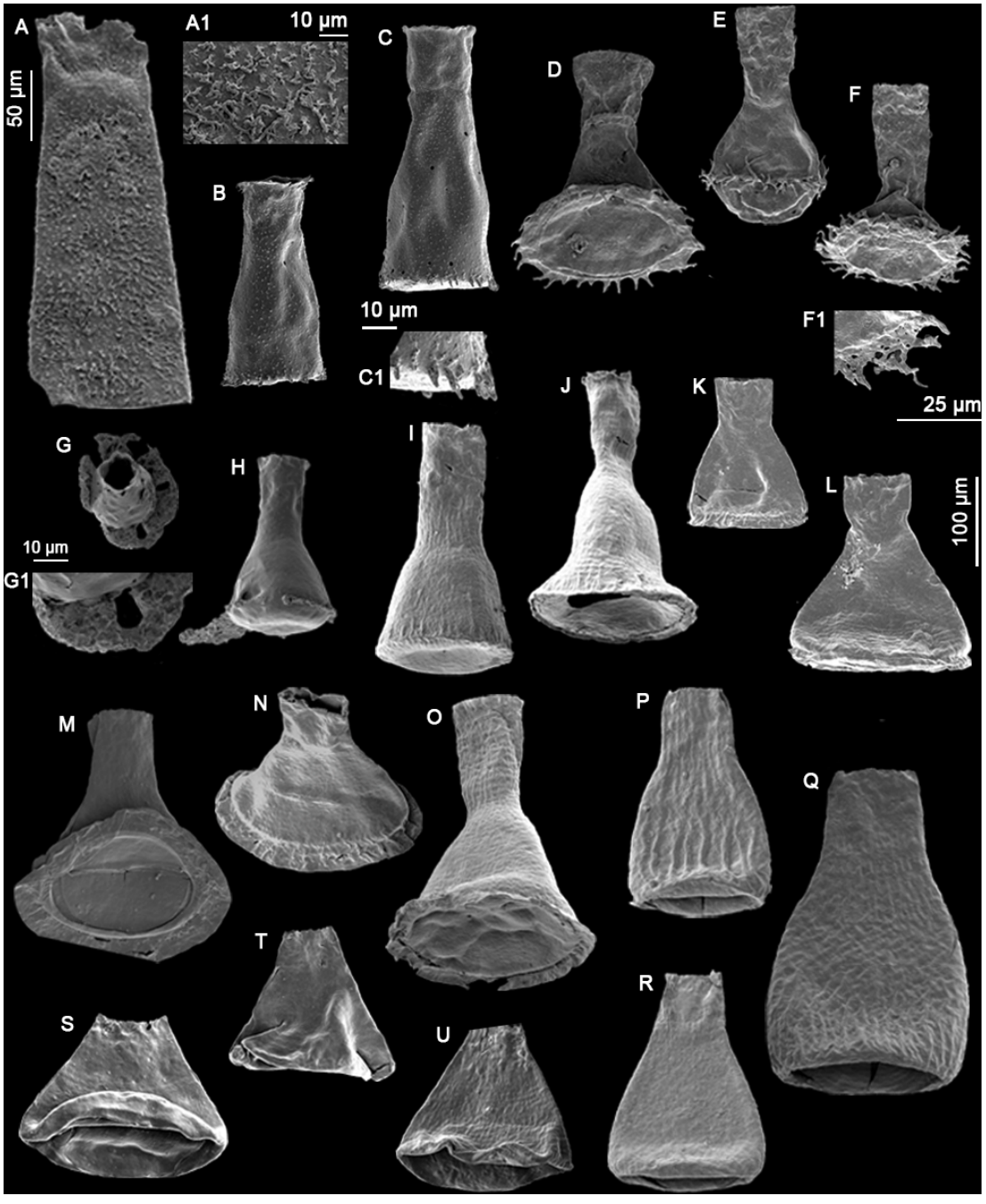


**Plate 2.** **(A)** *Belonechitina* sp. (GU33), **(A1)** detail view of the surface ornamentation (10 µm scale bar), **(B–C)** *Spinachitina* sp. A (TC3), **(C1)** detail view of the spines (10 µm scale bar), **(D–F)** *Anthochitina primula* Nestor (1994) (GU7, GU33, GU33), **(F1)** detail view of the carina structure (25 µm scale bar), **(G–H)** *Anthochitina admirabilis* n. sp. with specimen **(G)** as the holotype and specimen **(H)** as the paratype (LM40), **(G1)** detail view of the carina features (10 µm scale bar), **(I–J)** *Cyathochitina campanulaeformis* Eisenack (1931) (RT2), **(K–L)** *Cyathochitina caputoi* da Costa (1971) (C46), **(M–O)** *Cyathochitina kuckersiana* Eisenack (1934) (C46, C46, RT2), **(P–R)** *Cyathochitina macastyensis* Achab (1978) (GU33, GU1, GU33), and **(S–U)** *Cyathochitina triangula* n. sp. with specimen **(S)** as the holotype and specimens **(T)** and **(U)** as paratypes (C46, C46, C45). The 50 µm scale bar applies to specimens **(A)**–**(H)**, unless indicated differently. The right 100 µm scale bar is used for specimens **(I)**–**(R)**.

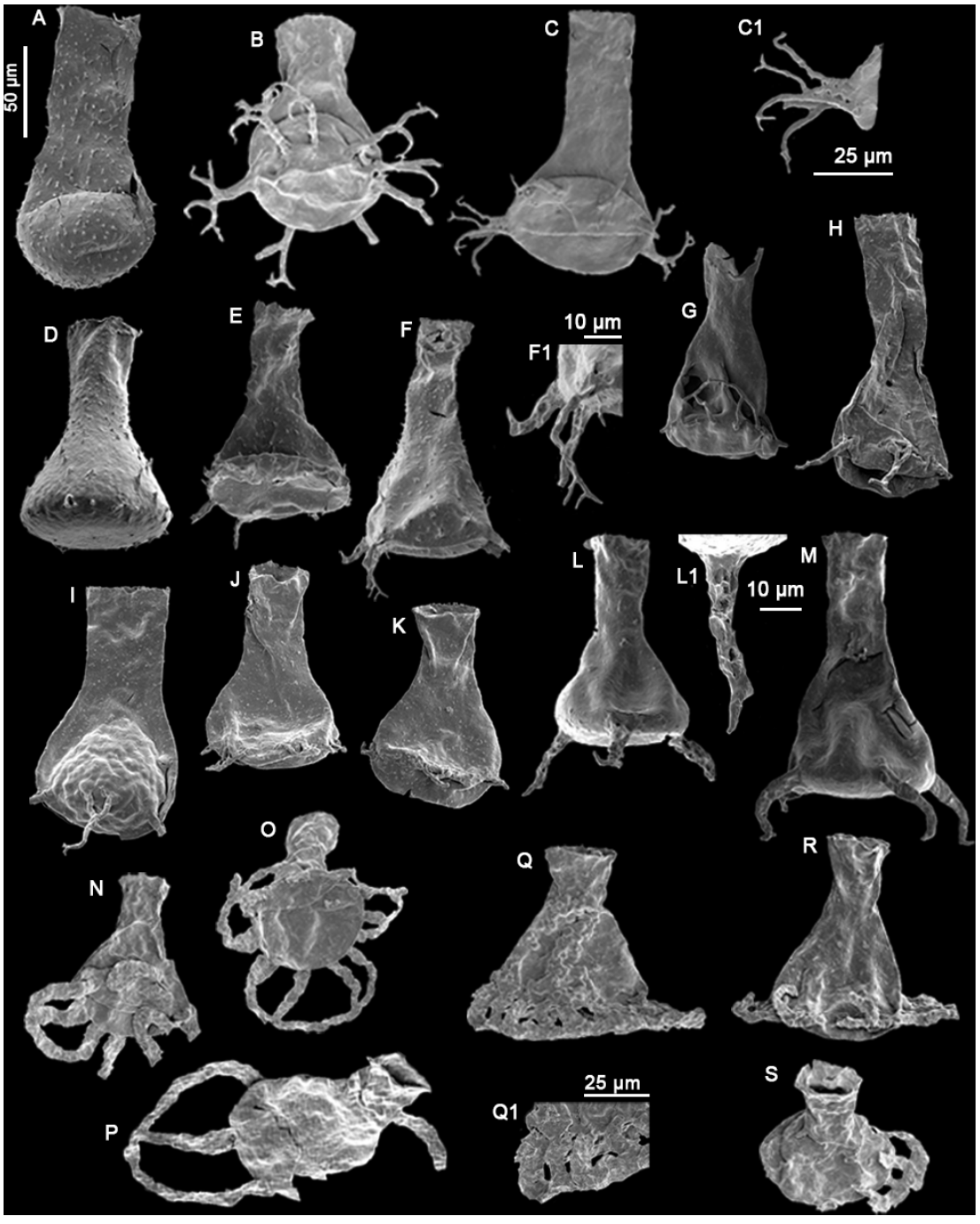


**Plate 3.** **(A)** *Angochitina* sp. A sensu Klock et al., 2024b (LM9), **(B–C)** *Ancyrochitina ramosaspina* Nestor (1994) (GU7, GU1), **(C1)** detail view of the processes (25 µm scale bar), **(D–F)** *Ancyrochitina wilsonae* Klock et al. (2024b) (LM60, RT5, RT5), **(F1)** detail view of the processes (10 µm scale bar), **(G)** *Clathrochitina perexilis* Soufiane and Achab (2000) (LM173), **(H–I)** *Clathrochitina postconcinna* Soufiane and Achab (2000) (C45), **(J–K)** *Clathrochitina* sp. A (C45), **(L–M)** *Plectochitina ralphi* Nestor (1994) (LM60), **(L1)** detail view of a process (10 µm), **(N–P)** *Plectochitina triplesiensis* n. sp. with specimen **(O)** as the holotype and specimens **(N)** and **(P)** as paratypes (TC5), **(Q–S)** *Plectochitina anulata* n. sp. with specimen **(Q)** as the holotype and specimens **(R)** and **(S)** as paratypes (TC5, TC6, TC5), and **(Q1)** detail view of the processes (25 µm scale bar). The 50 µm scale bar applies to all species, unless indicated differently.

et al. (2007) reported organic-walled green algae "disaster species" blooming during the carbon cycle perturbation associated with the Triassic–Jurassic mass extinction event, while the calcareous nannoplankton became malformed and extinct. Probably, a similar fundamental pathway lies at the base of the observed increased morphological disparity (i.e. diversity of morphotaxa) on the one hand and the increased amounts of teratology, which is an end member of morphological reaction to stress, on the other hand.

One could interpret the succession of *P. triplesiensis*, *P. anulata*, and *A. admirabilis* as an evolutionary lineage of increasing ornamental complexity. These three species have similar vesicle shapes but different ornaments: *P. triplesiensis* has 10 processes on average that are combined into different sets, while *P. anulata* has an average number of 20 processes that are all connected by one annular structure. In this hypothesis, *P. triplesiensis* may have started to develop more and more processes, with connected tips, which eventually evolved into another taxon, *P. anulata*. Both species have a similar stratigraphic range (Fig. 6). *A. admirabilis* could be interpreted as a next stage in a morphospecies evolutionary complex with *P. triplesiensis* and *P. anulata*, where many processes are now fused into a perforated carina. *A. admirabilis* appears higher than *P. triplesiensis* and *P. anulata* but disappears at the same level.

Alternatively, ecophenotypism could be at play. For instance, De Backer et al. (2024), in their study of chitinozoan responses to the Frasnian–Famennian Kellwasser events, emphasised that ornamental changes of morphologically otherwise similar forms during times of environmental stress may represent ecophenotypism rather than true evolutionary changes. In the case of *P. triplesiensis*, *P. anulata*, and *A. admirabilis*, the morphological disparity could also be due to ecophenotypism, where the processes and carina structure are expressed differently in response to a rapidly changing environment.

### 5.2 Local chitinozoan biozonation

The *A. ramosaspina* Local Biozone was originally defined by Soufiane and Achab (2000) using the total range of the index species. In their study, the base of the biozone is in their Member 4 (i.e. Macgilvray Member) of the Gun River Formation, which was the lowest sample analysed at the time. Although Soufiane and Achab (2000) interpreted the age of the Gun River Formation to be Rhuddanian, Copper and Jin (2015) revised this to the Aeronian. According to Soufiane and Achab (2000), *A. ramosaspina* occurs with *E. electa* and *C. gunriveris* at the base of the biozone. Throughout the biozone, it is associated with *C. edjelensis*, *B. basiconcava, Plectochitina* sp. 1, and *C.* cf. *proboscifera*.

In our studied sections, the *A. ramosaspina* Biozone is also recognised (Fig. 6). We find that the LO of *A. ramosaspina* is lower in the section than suggested by Soufiane and Achab (2000), as the taxon already appears in the lowest sample (C45) collected in the Merrimack Formation (Fig. 6). Therefore, following the original local biozone definition, the biozone is extended downward and has its base in the Merrimack Formation. Through the whole biozone, the index species is associated with *E. electa, B. praedolioliformis, C. caputoi, and C. gunriveris.* In addition to these species occurring in the local biozone mentioned above, *C. postconcinna*, *Clathrochitina* sp. A, *C. kuckersiana, C. macastyensis*, and *C. triangula* occur in the lower part of the biozone. In the upper half of the biozone, *C. perexilis, P. triplesiensis*, *P. anulata*, *C. edjelensis, B. basiconcava, C. emmastensis, C. iklaensis, C. praeproboscifera, C. campanulaeformis, P. ralphi, A. wilsonae*, *A. admirabilis*, *Spinachitina* sp. A, *Calpichitina* sp. A, *A. primula, Belonechitina* sp., and *Angochitina* sp. A occur (Fig. 6). Additionally, we revise the original top of the biozone, which is now extended to the top of the Ferrum Member of the Jupiter Formation, where the highest occurrence of the index species was documented by Klock et al. (2024b), just below the lowest occurrence of *E. dolioliformis* in the Jumpers Cliff section.

It would be possible to refine the biostratigraphic resolution by splitting the *A. ramosaspina* Local Biozone into two subzones. A lower subzone would be defined by the LOs of the suite of species at the top of the Menier Formation (TC 1 to TC 10), with a second subzone including *C. perexilis, P. triplesiensis*, *P. anulata*, *C. edjelensis, B. basiconcava, C. emmastensis, C. iklaensis, C. praeproboscifera, C. campanulaeformis, P. ralphi, A. wilsonae*, *A. admirabilis*, *Spinachitina* sp. A, *Calpichitina* sp. A, *A. primula, Belonechitina* sp., and *Angochitina* sp. A. However, we have opted not to subdivide the biozone to ensure consistency in biozonal nomenclature across various papers and studies (e.g. Klock et al., 2024b).

### 5.3 Composite section of Anticosti Island

The data obtained in this study have been integrated with the ranges of selected species from previous publications in the study area, including Achab (1977, 1978), Soufiane and Achab (2000), Achab et al. (2011), De Decker (2017), and Klock et al. (2024b) (Fig. 7). This composite provides an overview of the chitinozoan biostratigraphy from the Ordovician–Silurian boundary interval throughout the lower Silurian of Anticosti Island. Species were selected based on their occurrence in more than one paper and their importance related to the established local and global biozones. Our study fills an important gap in the chitinozoan biostratigraphic record of Anticosti Island between the Gun River and Chicotte formations (Fig. 7). Additionally, it confirms the stratigraphic potential of some species kept in open nomenclature by Soufiane and Achab (2000), which were placed in synonymy with our new species, e.g. *Plectochitina* sp. 1 with *P. triplesiensis* and *Plectochitina* sp. 2 with *P. anulata.*

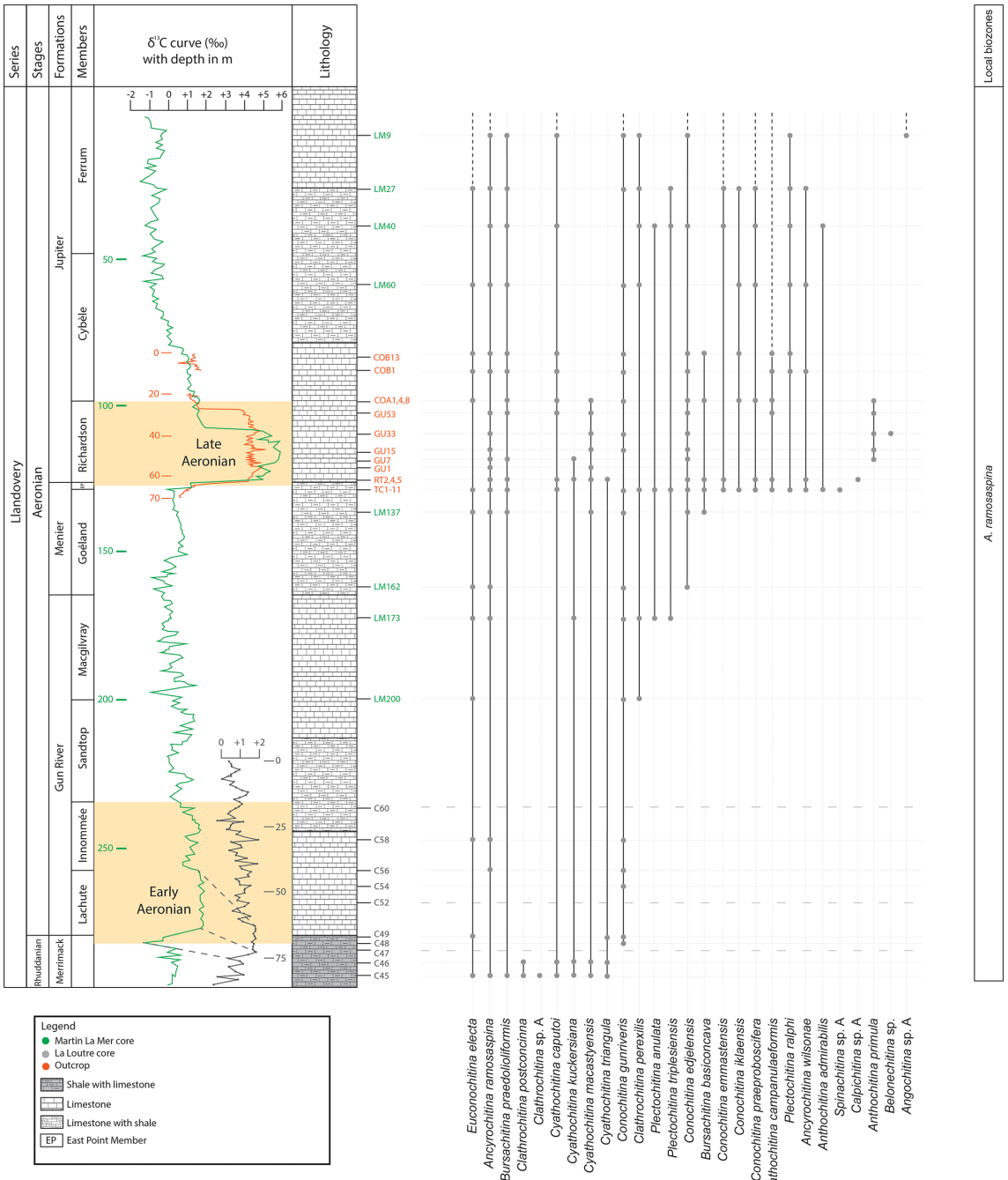


**Figure 6.** Composite log of the chitinozoan ranges, proposed biozone, and $\delta^{13}C$ data for the stratigraphic interval containing all studied samples. Composite produced based on the common lithostratigraphy in all sections. The $\delta^{13}C$ isotope curve from the Martin La Mer core and from the outcrop composite data is based on Braun et al. (2021), and the $\delta^{13}C$ isotope curve from the La Loutre core data on Daoust (2017). The vertical scale (in metres) is indicated next to each curve. Note that to use a single vertical scale, samples TC1-11, RT2,4,5, and COA1,4,8 contain multiple stratigraphically discrete samples but are only indicated by one line on this figure. See Figs. 2–4 for an extended zoom on this interval. A dashed line in the chitinozoan species range means that the same species are found in the younger sections of the Jupiter Formation and Chicotte Formation by Klock et al. (2024b). In the La Loutre core the CIE seems to start in the upper Rhuddanian, but that is an artefact of lithostratigraphically correlating both cores; dashed lines correlated to the curve of Braun et al. (2021) indicate a minor diachroneity between lithostratigraphic units in both locations.

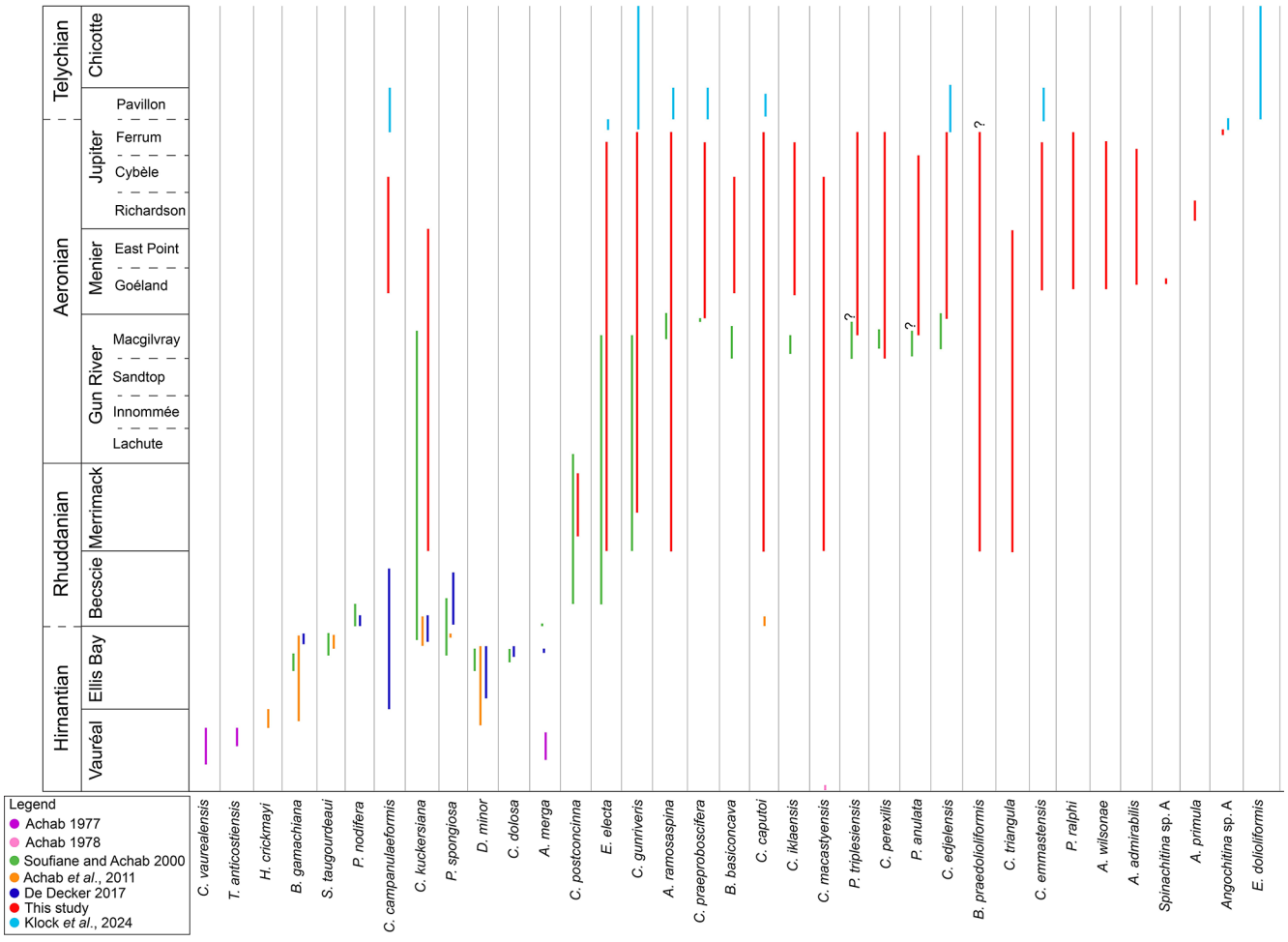


**Figure 7.** Summary figure of combined species ranges within Anticosti Island, from the Hirnantian (Ordovician) Vauréal Formation up to the Telychian (Silurian) Chicotte Formation. Species selected for comparison are based on common occurrences in multiple papers. Data used from Achab (1977, 1978), Soufiane and Achab (2000), Achab et al. (2011), De Decker (2017), and Klock et al. (2024b) and data obtained in this study. Synonymy applied includes *Plectochitina* sp. 1 sensu Soufiane and Achab (2000) with *P. triplesiensis* and *Plectochitina* sp. 2 sensu Soufiane and Achab (2000) with *P. anulata*.

### 5.4 Stratigraphic implications of *Bursachitina praedolioliformis* n. sp.

*Bursachitina praedolioliformis* n. sp. (Plate 4E–G) is created herein following the practice of Nestor (1994), who created *C. praeproboscifera* as an intermediary species between *C. iklaensis* and *C. proboscifera*. Nestor (1994) suggested that these three species could be related. Following this nomenclatural antecedent, *B. praedolioliformis* shows great resemblance to *E. dolioliformis* (Plate 4A–D), albeit lacking the characteristic spines (which somewhat artificially places it in the smooth genus *Bursachitina* rather than the ornamented genus *Eisenackitina*).

*B. praedolioliformis* in Anticosti Island ranges from the Rhuddanian Merrimack Formation through the Aeronian Gun River, Menier, and Jupiter formations (Plate 4) and lacks any wall ornamentation. Specimens observed by Davies et al. (2013) and Vandenbroucke et al. (2003), from the Type Llandovery area in Wales and the Girvan District in Scotland, respectively, were originally attributed to *E. dolioliformis* but lacked wall ornamentation, with the rare exception of sparsely distributed granules on the vesicles of some of the Welsh specimens. The Welsh and Scottish specimens generally have the typical subcylindrical vesicle shape and size of *E. dolioliformis* and its thick walls, but given the lack of clear ornamentation, we propose that they should be reassigned to *B. praedolioliformis* n. sp. In terms of stratigraphic occurrence, the specimens from the Type Llandovery area are from the upper Aeronian (Davies et al., 2013), and the Scottish glabrous specimens range from the *S. sedgwickii* graptolite zone in the upper Aeronian to the *M. griestoniensis* graptolite zone in the lower to middle Telychian (Vandenbroucke et al., 2003). In contrast, the ornamented *E. dolioliformis* holotype was reassigned to a Telychian age (Jacques Verniers, per-

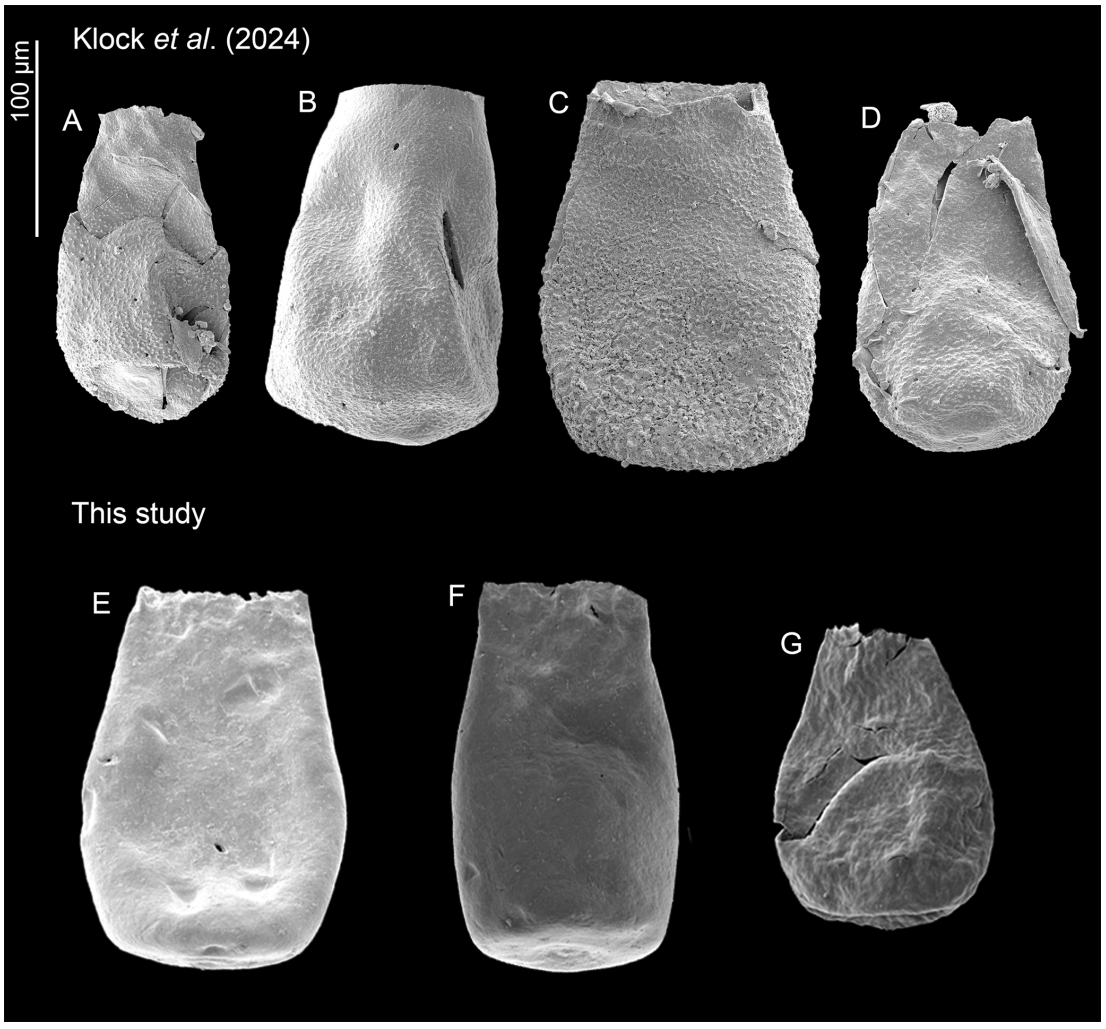


**Figure 8.** Overview of the ornamented *Eisenackitina dolioliformis* and smooth new species *Bursachitina praedolioliformis* specimens. **(A–D)** *E. dolioliformis* analysed and identified by Klock et al. (2024b) and **(E–G)** *B. praedolioliformis* n. sp. from this study.

sonal communication, 2024), and the species has been consistently described in Telychian aged units from the Baltic area (e.g. Nestor, 1994, 2012; Loydell et al., 2010; Männik et al., 2015).

As such, *B. praedolioliformis* would be characteristic of the upper Rhuddanian to the lower Telychian stages (this study, Vandenbroucke et al., 2003; Davies et al., 2013), whereas typical *E. dolioliformis* would be constrained to the Telychian.

The substantial number of specimens (145) found here adds significance to these observations. Plate 4 compares *E. dolioliformis* as found by Klock et al. (2024b) (Plate 4A–D) and the new species *B. praedolioliformis* found in this study (Plate 4E–G).

### 5.5 Global correlation and chronostratigraphy

Verniers et al. (1995) established global chitinozoan biozones for the Silurian. Most of the Llandovery chitinozoan biozones are based on studies in the Baltic area. The global biozones that correspond to our studied interval are, from bottom to top, the *E. electa*, *S. maennili*, and *C. alargada* biozones. In our study area, only the index species *E. electa* is present (Fig. 8). Additionally, hardly any of the accompanying species of the biozones as defined by Verniers et al. (1995) occur in our study. Consequently, in the absence of the index species, the global biozonal scheme could not be directly applied to the Anticosti succession. The *A. ramosaspina* Local Biozone from Soufiane and Achab (2000) was used, which is defined by the total range of the marker species, and spans through our whole study section (Fig. 8). It should be noted that *C. alargada* as defined by Cramer (1967) is not recognised in the samples studied here.

However, *C. alargada* looks very similar to *C. iklaensis* as defined by Nestor (1980), and this species occurs in our study within the upper half of the *A. ramosaspina* Biozone. The definition of *C. alargada* (Cramer, 1967) is in need of revision, and no photographs are available that indicate how it differs from *C. iklaensis* (Nestor and Nestor, 2002; Hints et al., 2006). This hampers a clear differentiation between these two species, although based on the detailed description of *C. iklaensis*, we can be confident about our taxonomic assignment. *C. iklaensis* is an accompanying species of the *C. alargada* Biozone, which could indicate the start of this global biozone (sensu Verniers et al., 1995) in Anticosti Island; however, this cannot be affirmed solely based on the presence of *C. iklaensis*, as the species is known to range from the mid-Rhuddanian to the lower Telychian (Nestor, 2012).

The *A. ramosaspina* Local Biozone, as defined by Soufiane and Achab (2000), is extended downward to the top of the Merrimack Formation and upward to the Ferrum Member in the Jupiter Formation, indicating an age range from the late Rhuddanian to the late Aeronian. This biozone can be correlated globally: the species was first defined by Nestor (1994) in the Baltic area, correlating it to the global *S. maennili* Zone. The *E. electa* Partial Range Biozone as established by Soufiane and Achab (2000) is reduced and ranges from the Becscie Formation to the middle Merrimack Formation.

Copper and Jin (2012) defined the Gun River Formation to be early through mid-Aeronian in age and the Menier Formation as middle to late Aeronian, based on the underlying mid-Aeronian upper Macgilvray Member of the Gun River Formation that has the First Appearance Datums (FADs) of *Kulumbella* and *Pentamerus*. The reefs of the East Point Member are dated as late Aeronian. For the Jupiter Formation on Anticosti Island, Riva and Petryk (1981) reported the graptolite *Stimulograptus sedgwickii* in the Richardson Member, dating this member to the late Aeronian. Jin and Copper (2000) described the brachiopods *Stricklandia gwelani* and *S. planirostrata* from the Cybèle and Ferrum members; however, these brachiopod species failed to provide a definitive age in the absence of *Stricklandia lens*. They based the late Aeronian to early Telychian age of these two units on the occurrence of the *Stricklandia* species above the *S. sedgwickii* graptolite level. Zhang and Barnes (2002) discussed the occurrence of *Ozarkodina aldridgei* in the Jupiter Formation starting from the previous fourth member (now Cybèle Member) and correlated it with the global *Distomodus staurognathoides* Biozone, assigning a late Aeronian to early Telychian age to this part of the Jupiter Formation. Munnecke and Männik (2009) also reported the conodont *Ozarkodina* cf. *aldridgei* in the Pavillon Member. *Costistricklandia* brachiopods, however, indicate a Telychian age for the Pavillon Member and the Chicotte Formation (Jin and Copper, 2000; Copper and Jin, 2015). Considering these studies and a typical Aeronian chitinozoan assemblage in the Ferrum Member, Klock et al. (2024b) suggested the placement of the Aeronian–Telychian boundary between the Ferrum and Pavillon members. Furthermore, they found *E. dolioliformis* in the Pavillon Member and in the Chicotte Formation, a typical Telychian chitinozoan species, which agrees with the relative age provided by brachiopod and conodont data. In this study, the species *B. praedolioliformis* is observed from the late Rhuddanian (Merrimack Formation) to the end of the Aeronian (Ferrum Member) on Anticosti Island. In establishing this new species, the *E. dolioliformis* specimens found in Vandenbroucke et al. (2003) and Davies et al. (2013) are reclassified as *B. praedolioliformis*. This adds to Klock et al.'s (2024b) suggestion that *E. dolioliformis* is a typical Telychian species, as no specimens remain in the Aeronian. Based on our data and published occurrences by Davies et al. (2013) and Vandenbroucke et al. (2003), *B. praedolioliformis* occurs from the upper Rhuddanian to the lower Telychian.

## 6 Conclusions

The 42 studied samples yielded 9005 chitinozoan specimens, allowing for a robust calibration of the Llandovery biostratigraphy on Anticosti Island, with a special focus on biogeochemical events. We filled the gap in the biostratigraphic record for the Merrimack to Jupiter formations between the well-established Ordovician–Silurian boundary units and the younger Llandovery Jupiter and Chicotte formations studied by Klock et al. (2024b). The *A. ramosaspina* Local Biozone, as defined by Soufiane and Achab (2000), is extended downward to the top of the Merrimack Formation and upward to the top of the Ferrum Member. It comprises 27 species, including five newly defined species: *B. praedolioliformis*, *C. triangula*, *P. triplesiensis*, *P. anulata*, and *A. admirabilis*. The new species *B. praedolioliformis* concerns smooth specimens and excludes these from the spiny *E. dolioliformis*, the index species of the stratigraphically higher biozone. We suggest that *B. praedolioliformis* ranges from the uppermost Rhuddanian to the lower Telychian, while *E. dolioliformis* is restricted to the Telychian.

From sampling at the onset of and during the events, it can be concluded that the environmental changes that characterise the Silurian biogeochemical events had a remarkable impact on the chitinozoan assemblages. However, chitinozoans show different behaviours throughout the two studied carbon isotope excursion events. Although there are barren samples that render the conclusions less significant, several chitinozoan taxa disappear in the early Aeronian event but reappear in higher units. At the onset of the late Aeronian event, remarkable radiation is observed, where diverse ornamented species occur over a short time span. Additionally, this event features some characteristic, short-ranging (possibly disaster?) species that only exist during the event itself. Chitinozoans appear to have adapted their morphologies to

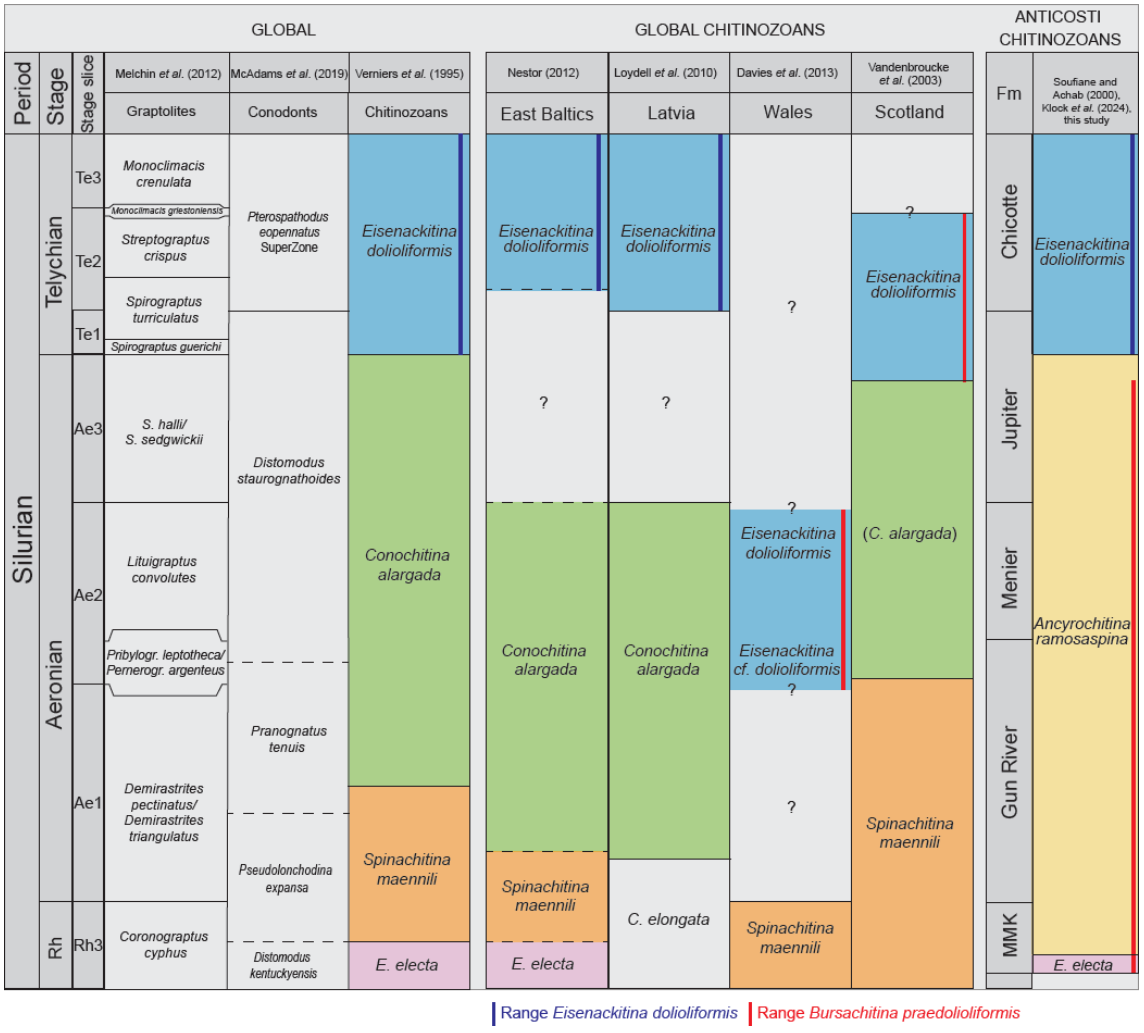


**Figure 9.** Correlation of combined Anticosti data with global graptolite, conodont, and chitinozoan biozones and other key areas in Llandovery. Graptolite data from Melchin et al. (2012), conodonts from McAdams et al. (2019), chitinozoans from Verniers et al. (1995), East Baltic area chitinozoans from Nestor (2012), Latvian chitinozoans from Loydell et al. (2010), Welsh chitinozoans from Davies et al. (2013), Scottish chitinozoans from Vandenbroucke et al. (2003), and Anticosti chitinozoan data from this study, Soufiane and Achab (2000), and Klock et al. (2024b). This schematic diagram is not to scale. In the East Baltic area and Latvia, the *E. dolioliformis* Biozone corresponds with the upper *S. turriculatus* and *M. crenulata* graptolite zones (Loydell et al., 2003, 2010). However, the base of the *E. dolioliformis* Biozone in correlation to the graptolite biozonation is unknown, due to a stratigraphic gap in the East Baltic sections (Loydell et al., 2010). In Scotland, this biozone correlates to the upper *S. sedgwickii* up to the lowest *M. griestoniensis* graptolite biozones (Vandenbroucke et al., 2003). In Anticosti, the *E. dolioliformis* Biozone spans the *S. guerichi* to the *M. crenulata* graptolite biozones. The *C. alargada* Biozone can be correlated with the middle to upper *D. triangulatus* through the top of the *L. convolutus* graptolite biozones in the East Baltic and Latvia (Loydell et al., 2010; Nestor, 2012). In Scotland, *C. alargada* is correlated to the upper half of the *P. leptotheca* Biozone up to the upper *S. sedgwickii* Biozone (Vandenbroucke et al., 2003). In Wales, *E. dolioliformis* is linked to the upper *L. convolutus* graptolite biozone and *E*. cf. *dolioliformis* to the *P. leptotheca* graptolite biozone (Davies et al., 2013). As noticeable in Fig. 8, this Welsh zone occurs lower in the stratigraphy than in the other localities where *E. dolioliformis* occurs. This confirms the differentiation of *B. praedolioliformis* from *E. dolioliformis,* where *B. praedolioliformis* occurs within the upper Rhuddanian to the lower Telychian, and *E. dolioliformis* would be constrained to the Telychian. The *S. maennili* Biozone in the East Baltic is correlated with the upper *C. cyphus* and lower *D. triangulatus* graptolite biozones (Nestor, 2012). In Wales, *S. maennili* is found in what was a Global Boundary Stratotype Section and Point (GSSP) candidate for the base of the Aeronian (Melchin et al., 2023), while in Scotland, it spans the *C. cyphus* to the lower *P. leptotheca* graptolite biozones (Vandenbroucke et al., 2003). In Latvia, the *C. elongata* Biozone is correlated to the upper *C. cyphus* and lower *D. triangulatus* graptolite biozones (Loydell et al., 2010). In the East Baltic, the *E. electa* Biozone is correlated with the middle to upper part of the *C. cyphus* graptolite biozone (Loydell et al., 2003, 2010).

the changing environmental conditions during the biogeochemical event, but no extinction of taxa is observed.

## Appendix A: Numerical overview of chitinozoan taxa extracted from the 42 samples

**Table A1.** Overview table with the number of chitinozoans counted per taxon in the 42 samples. Right column: bold indicates the productive samples yield around 300 chitinozoan specimens, italic indicates the moderately productive samples, and normal font indicates the barren samples. Lower row: bold indicates very abundant species, italic indicates moderately present species, and normal font indicates species in low abundance and taxa identified to the genus level.

| Sample site | Sample name | Geological unit | *Euconochitina electa* | *Ancyrochitina* | *cancassajina* | *Bursachitina* | *praedolioliformis* | *Clathrochitina* | *postconanna* | *Clathrochitina* sp. A | *Cyathochitina caputa* | *Cyathochitina* | *kuckersiana* | *Cyathochitina* | *macalpensis* | *Cyathochitina triangula* | *Conochitina guerinensis* | *Clathrochitina perexilis* | *Plectochitina* | *triplesiensis* | *Plectochitina amulata* | *Conochitina eljelensis* | *Bursachitina basiconcava* | *Conochitina emmonsensis* | *Conochitina iklaensis* | *Conochitina* | *praeprobosifera* | *Cyathochitina* | *campanulaeformis* | *Plectochitina ralphi* | *Ancyrochitina wilsoniae* | *Anthochitina adnivirabilis* | *Spinachitina* sp. A | *Calpichitina* sp. A | *Anthochitina pennula* | *Belonechitina* sp. | *Angochitina* sp. A | *Ancyrochitina* spp | *Bursachitina* spp | *Calpichitina* spp | *Clathrochitina* spp | *Conochitina* spp | *Cyathochitina* spp | *Plectochitina* spp | Chitinozoa indet | Total |
|---|---|---|---|---|---|---|---|---|---|---|---|---|---|---|---|---|---|---|---|---|---|---|---|---|---|---|---|---|---|---|---|---|---|---|---|---|---|---|---|---|---|---|---|---|---|---|
| Martin La Mer core | LM9 | Jupiter Fm - Ferrum Mb | | 79 | 4 | | | | | | 4 | | | | | | 3 | 1 | | | 5 | | | | | | | | 27 | | | | | | | 7 | 100 | | | 15 | | 11 | 28 | **284** |
| | LM27 | | 10 | 20 | 9 | | | | | | | | | | | | 14 | 3 | 1 | | | 5 | | 1 | 3 | 1 | | | 4 | 1 | | | | | | | 91 | | 1 | 24 | | 27 | 67 | **277** |
| | LM40 | | | 36 | 7 | | | | | | 6 | | | | | | | 1 | 13 | 5 | 3 | | | 1 | | 1 | | | 3 | | 23 | | | | | | 25 | | 2 | 13 | 13 | 50 | 40 | **242** |
| Jupiter coastal section | LM60 | Jupiter Fm - Cybèle Mb | 3 | 52 | 2 | | | | | | | | | | | | 1 | 1 | | | | | | | 1 | 1 | | | 81 | 1 | | | | | | | 40 | | | 9 | 4 | 54 | 27 | **277** |
| | COB13 | | 37 | 4 | 1 | | | | | | 1 | | | | | | 25 | | | | | 82 | | | 3 | | 6 | | 8 | | | | | | | | 1 | | 29 | 81 | 12 | | 14 | **304** |
| | COB1 | | 33 | 12 | 2 | | | | | | 1 | | | | | | 29 | | | | | 53 | | | | | 5 | | 1 | 1 | | | | | | | 1 | | 1 | 18 | 116 | 18 | 1 | 8 | **300** |
| | COA8 | | 4 | | 13 | | | | | | | | | | 11 | | 60 | | | | | 34 | 56 | | 1 | 11 | 4 | | | | | | | | | | | | | | 72 | 11 | 2 | 14 | **293** |
| | COA4 | | 2 | | 14 | | | | | | 2 | | | | 4 | | 94 | | | | | 113 | 2 | | | 4 | 3 | | | | | | | | | | | | | | 50 | 7 | | 1 | **296** |
| | COA1 | | 5 | | 5 | | | | | | | | | | 1 | | 85 | | | | | 80 | 1 | | 2 | 3 | 2 | | | | | | | | 1 | | | | | | 83 | 1 | | 24 | **293** |
| | GU53 | Jupiter Fm - Richardson Mb | | 57 | 1 | | | | | | 1 | | | | 3 | | | | | | | 1 | | | | | 20 | | | | | | | | 7 | | | 16 | | 40 | 1 | 24 | 22 | 61 | **254** |
| | GU33 | | | 32 | | | | | | | | | | | 9 | | 2 | | | | | 6 | | | | | 1 | | | | | | | | 1 | | | 31 | | 2 | 42 | 1 | 1 | 3 | 24 | **239** |
| | GU15 | | | 56 | | | | | | | | | | | 1 | | 5 | | | | | 6 | | | | | | | | | | | | 63 | | | 23 | | | 46 | 4 | 1 | | 90 | **295** |
| | GU7 | | | 14 | 1 | | | | | | | | 3 | | | | | | | | | 1 | | | | | | | | | | | | 209 | | | 19 | | 1 | 9 | | 2 | | 28 | **287** |
| | GU1 | | | 222 | | | | | | | | | | | 6 | | | | | | | | | | | | | | | | | | | | | 63 | | | | | 1 | | 23 | **315** |
| | RT5 | | | 37 | 1 | | | | | | 4 | | 6 | | 1 | | | | | | | 5 | | 7 | | 4 | | | 11 | | | 2 | | | | 21 | | | 68 | 7 | 17 | 4 | 78 | **273** |
| | RT4 | | | 22 | 32 | | | | | | 6 | | 5 | | 5 | 11 | | | | | | 7 | 3 | 3 | | 80 | 14 | | | | | | | | | 13 | 2 | | 12 | 32 | 23 | | 30 | **300** |
| | RT2 | | | 20 | | | | | | | 21 | | 13 | | 7 | 3 | | | | | | 1 | | 2 | | 2 | 14 | | | | | | | | | 4 | | | 92 | 6 | 15 | 32 | 43 | **275** |
| | TC1 | Menier Fm - East Point Mb | | | | | | | | | | | | | | | | | | | | | | | | | | | | | | | | | | | | | | 3 | | 1 | 4 | 8 |
| | TC2 | Menier Fm - Goéland Mb | 1 | | 1 | | | | | | | | | | | | 3 | | | | | 7 | | 1 | 1 | | | | | | | | | | | | | | | 7 | | 1 | 11 | 33 |
| | TC3 | | 45 | 37 | 1 | | | | | | | | | | | | 27 | | 1 | 2 | 68 | 3 | | 6 | | | | | | | | 6 | | | | 12 | | | | 60 | | 18 | 8 | **294** |
| | TC4 | | 14 | 10 | 9 | | | | | | | | | | | | 20 | | | 3 | 70 | 12 | | 10 | 1 | | | 1 | | 2 | | | | | 3 | | | | 57 | 1 | 5 | 74 | **292** |
| | TC5 | | 2 | 10 | 1 | | | | | | | | | | | | 13 | | 23 | 11 | 37 | 6 | | 3 | 3 | 1 | 2 | | | | | | | | 19 | | | 2 | 62 | | 34 | 44 | **273** |
| | TC6 | | 15 | 13 | 1 | | | | | | | | | | | | 18 | | 1 | 2 | 43 | 6 | | 17 | 1 | | 1 | 3 | | | | | | | 8 | | | | 24 | | 11 | 69 | **233** |
| | TC7 | | 99 | 2 | | | | | | | | | | | | | 1 | 2 | | | 31 | | 1 | 71 | 1 | | 2 | 1 | | | | | | | 2 | | | | 64 | | 1 | 10 | **288** |
| | TC8 | | 159 | 3 | | | | | | | | | | | | | | | 1 | | 19 | | 1 | 22 | 2 | | | | | | | | | | 1 | | | | 47 | | 8 | 34 | **297** |
| | TC9 | | 3 | 25 | 21 | | | | | | | | | | | | 1 | | | | 6 | 1 | 22 | 18 | 23 | 2 | 13 | | | | | | | | 27 | | | | 46 | 1 | 23 | 40 | **272** |
| | TC10 | | | 56 | 10 | | | | | | 21 | | | | | | 9 | | | | 14 | | | 9 | 32 | | | | | | | | | | 59 | | | | 24 | 7 | | 46 | **287** |
| | TC11 | | 4 | 103 | | | | | | | 1 | | | | | | 29 | | | | 8 | 7 | | | | | | | | | | | | | 64 | | | | 49 | | | 17 | **282** |
| Martin La Mer core | LM137 | | 3 | 60 | 7 | | | | | | | | | | 1 | | 53 | | | | 38 | 12 | | | | | | | | | | | | | 32 | | | | 60 | 1 | | 8 | **275** |
| | LM162 | | 1 | 99 | | | | | | | | | | | | | 23 | | | | 12 | | | | | | | | | | | | | | 114 | | | 1 | 14 | | | 16 | **280** |
| | LM173 | Gun River Fm - Macgilvray Mb | 2 | 19 | | | | | | | | | 9 | | | | 4 | 78 | 1 | 1 | | | | | | | | | | | | | | | 38 | | | 96 | 8 | 2 | | 16 | **274** |
| | LM200 | | 19 | | | | | | | | | | | | | | 41 | 1 | | | | | | | | | | | | | | | | | 4 | | | 2 | 18 | 3 | | 15 | *103* |
| La Loutre #1 drillcore | C60 | Gun River Fm - Innommée Mb | | | | | | | | | | | | | | | | | | | | | | | | | | | | | | | | | | | | | | | | | | 0 |
| | C58 | | 5 | 2 | | | | | | | | | | | | | 10 | | | | | | | | | | | | | | | | | | 18 | | | 5 | 4 | | | 22 | 66 |
| | C56 | Gun River Fm - Lachute Mb | | 48 | | | | | | | | | | | | | 1 | | | | | | | | | | | | | | | | | | 30 | | | 1 | 2 | | 8 | 11 | *101* |
| | C54 | | | | | | | | | | | | | | | | 2 | | | | | | | | | | | | | | | | | | | | | | | | | | | 2 |
| | C52 | | | | | | | | | | | | | | | | | | | | | | | | | | | | | | | | | | | | | | | | | | 4 | 4 |
| | C49 | Merrimack Fm | 4 | | | | | | | | | | | | | 1 | 22 | | | | | | | | | | | | | | | | | | 19 | | | | | | 14 | 34 | *94* |
| | C48 | | | | | | | | | | | | | | | | 1 | | | | | | | | | | | | | | | | | | | | | | | | | | 2 | 3 |
| | C47 | | | | | | | | | | | | | | | | | | | | | | | | | | | | | | | | | | 5 | | | | 1 | | 1 | 2 | 9 |
| | C46 | | | | | | | 3 | | | 22 | | 50 | | 3 | 9 | | | | | | | | | | | | | | | | | | | 35 | | | 6 | 2 | 49 | 5 | 47 | **231** |
| | C45 | | 3 | 7 | 2 | | 17 | 7 | 13 | | 17 | | 1 | | 17 | | | | | | | | | | | | | | | | | | | 31 | | | 12 | 1 | 21 | 5 | 46 | **200** |
| | | | **473** | **1157** | *145* | | *20* | *7* | *103* | | *103* | | *53* | | *41* | | **593** | *87* | *41* | *24* | **746** | *109* | *45* | *167* | *171* | | *72* | *143* | | *18* | *25* | *6* | *2* | **364** | *1* | *7* | 969 | *2* | *4* | 484 | 1067 | 235 | 341 | 1180 | 9005 |

## Appendix B: Alphabetical list of all chitinozoan species recognised in this material

*Ancyrochitina ramosaspina*

*Ancyrochitina wilsonae*

*Angochitina* sp. A

*Anthochitina admirabilis* n. sp.

*Anthochitina primula*

*Belonechitina* sp.

*Bursachitina basiconcava*

*Bursachitina praedolioliformis* n. sp.

*Calpichitina* sp. A

*Clathrochitina perexilis*

*Clathrochitina postconcinna*

*Clathrochitina* sp. A

*Conochitina edjelensis*

*Conochitina emmastensis*

*Conochitina gunriveris*

*Conochitina iklaensis*

*Conochitina praeproboscifera*

*Cyathochitina campanulaeformis*

*Cyathochitina caputoi*

*Cyathochitina kuckersiana*

*Cyathochitina macastyensis*

*Cyathochitina triangula* n. sp.

*Euconochitina electa*

*Plectochitina anulata* n. sp.

*Plectochitina ralphi*

*Plectochitina triplesiensis* n. sp.

*Spinachitina* sp. A

**Data availability.** All chitinozoan data used in this paper are included in Table A1. Holotypes of the new species can be accessed at the Royal Belgian Institute of Natural Sciences in Brussels (collection numbers are IRSNB b10053–b10067).

**Author contributions.** Conceptualisation: CK, AD, and TRAV. Funding acquisition: CK, TRAV, and AD. Sample collection: FMRJ, CK, AD, and PD. Species identification discussions: FMRJ, CK, and TRAV. Writing: FMRJ, CK, and TRAV, with contributions from AD and PD.

**Competing interests.** The contact author has declared that none of the authors has any competing interests.

**Disclaimer.** Publisher's note: Copernicus Publications remains neutral with regard to jurisdictional claims made in the text, published maps, institutional affiliations, or any other geographical representation in this paper. While Copernicus Publications makes every effort to include appropriate place names, the final responsibility lies with the authors.

**Acknowledgements.** Field campaigns for Carolina Klock and Fien Jonckheere were supported by the research incubator of the Société du Patrimoine Mondial Anticosti. Carolina Klock and Thijs Vandenbroucke received funding from the Human Frontier Science Program (HFSP; grant RGP0066/2021). Thijs Vandenbroucke acknowledges funding by the Research Foundation–Flanders (research grant G038722N, Monsters of the Apocalypse) and the King Baudouin Foundation (Professor T. Van Autenboer Fund). Chitinozoan SEM images were generated using research infrastructure funded through FWO grant I013118N. The authors also acknowledge Jacques Verniers and Tim De Backer for help with chitinozoan species identifications and feedback, Patrick McLaughlin and Poul Emsbo for discussions on event stratigraphy, and Matthew Braun for discussions on Anticosti Island chemostratigraphy, as well as assistance in the field. We thank Sabine Van Cauwenberghe for assistance with the lab preparations. Sonia Camina and Anthony Butcher provided insightful review, for which we are grateful.

**Financial support.** This research has been supported by the Human Frontier Science Program (grant no. RGP0066/2021), the Fonds Wetenschappelijk Onderzoek (grant nos. G038722N and I013118N), and the King Baudouin Foundation United States (Professor T. Van Autenboer Fund).

**Review statement.** This paper was edited by Luke Mander and reviewed by Sonia Clara Camina and Anthony Butcher.

## References

Achab, A.: Les chitinozoaires de la zone à *Dicellograptus complanatus* Formation de Vauréal, Ordovicien supérieur, Ile d'Anticosti, Québec, Can. J. Earth. Sci., 14, 413–425, 1977.

Achab, A.: Sur Quelques Chitinozoaires de la Formation de Vauréal et de la Formation De Macasty (Ordovicien Supérieur), Ile d'Anticosti, Québec, Canada, Rev. Palaeobot. Palyno., 25, 295–314, 1978.

Achab, A.: Biostratigraphie par les Chitinozoaires de l'Ordovicien Supérieur-Silurien Inférieur de l'Ile d'Anticosti, Résultats préliminaires, in: Field meeting, Anticosti-Gaspé, Québec, II: Stratigraphy and Paleontology, edited by: Lespérance, P. J., Subcommission on Silurian Stratigraphy and Ordovician-Silurian Boundary Working Group, Montreal, 143–157, 1981.

Achab, A., Asselin, E., Desrochers, A., Riva, J. F., and Farley, C.: Chitinozoan biostratigraphy of a new Upper Ordovician stratigraphic framework for Anticosti Island, Canada, Bull. Geol. Soc. Am., 123, 186–205, https://doi.org/10.1130/B30131.1, 2011.

Achab, A., Asselin, E., Desrochers, A., and Riva, J. F.: The end-Ordovician chitinozoan zones of Anticosti Island, Québec: Definition and stratigraphic position, Rev. Palaeobot. Palyno., 198, 92–109, https://doi.org/10.1016/j.revpalbo.2012.07.019, 2013.

Barnes, C. R.: Stratigraphy and Palaeontology of the Ordovician-Silurian boundary interval, Anticosti Island, Quebec, Canada, Bull. Br. Museum Nat. Hist. Geol., 43, 195–219, 1988.

Bengtson, P.: Open Nomenclature, Palaeontology, 31, 223–227, 1988.

Bordet, E., Malo, M., and Kirkwood, D., A structural study of western Anticosti island, St. Lawrence platform, Quebec: a fracture analysis that integrates surface and subsurface structural data, Bull. Can. Petrol. Geol., 58, 36–55, https://doi.org/10.2113/gscpgbull.58.1.36, 2010.

Braun, M. G., Daoust, P., and Desrochers, A.: A sequential record of the Llandovery $\delta^{13}C_{carb}$ excursions paired with time-specific facies: Anticosti Island, eastern Canada, Palaeogeo, 578, 110566, https://doi.org/10.1016/J.PALAEO.2021.110566, 2021.

Calner, M.: Silurian global events – at the tipping point of climate change, in: Mass extinction, edited by: Elewa, A. M. T., Springer, 21–58, e-ISBN: 978-3-540-75915-7, 2008.

Clayer, F. and Desrochers, A.: The stratigraphic imprint of a mid-Telychian (Llandovery, early Silurian) glaciation on far-field shallow-water carbonates, Anticosti Island, Eastern Canada, Est. J. Earth Sci., 63, 207–213, https://doi.org/10.3176/earth.2014.20, 2014.

Copper, P. and Jin, J.: Early Silurian (Aeronian) East Point Coral Patch Reefs of Anticosti Island, Eastern Canada: First Reef Recovery from the Ordovician/ Silurian Mass Extinction in Eastern Laurentia, Geosciences, 2, 64-89, https://doi.org/10.3390/geosciences2020064, 2012.

Copper, P. and Jin, J.: The revised lower Silurian (Rhuddanian) Becscie formation, Anticosti island, eastern Canada records the tropical marine faunal recovery from the end-Ordovician mass extinction, Newsl. Stratigr., 47, 61–83, https://doi.org/10.1127/0078-0421/2014/0040, 2014.

Copper, P. and Jin, J.: Tracking the early Silurian post-extinction faunal recovery in the Jupiter Formation of Anticosti Island, eastern Canada: A stratigraphic revision, Newsl. Stratigr., 48, 221–240, https://doi.org/10.1127/nos/2015/0061, 2015.

Copper, P. and Long, D. G. F.: Stratigraphic revisions for a key Ordovician/Silurian boundary section, Newsl. Stratigr., 21, 59–73, 1989.

Copper, P. and Long, D. G. F.: Stratigraphic revision of the Jupiter Formation, Anticosti Island, Canada: a major reference section above the Ordovician-Silurian boundary, Newsl. Stratigr., 23, 11–36, https://doi.org/10.1127/nos/23/1990/11, 1990.

Copper, P., Long, D. G. F., and Jin, J.: The early Silurian Gun River Formation of Anticosti Island, eastern Canada: A key section for the mid-Llandovery of North America, Newsl. Stratigr., 45, 263–280, https://doi.org/10.1127/0078-0421/2012/0024, 2012.

Cramer, F. H.: Microplankton from three Paleozoic formations in the Province of León (NW Spain), Leidse Geologische Mededelingen, 30, 255–361, 1964.

Cramer, F. H. and Diez, M. d. C. R.: Iberian Chitinozoans. I. Introduction and Summary of Pre-Devonian Data. Palinologia, num. extraord, 1, 149–202, León, 1978.

Cramer, B. D., Brett, C. E., Melchin, M. J., Männik, P., Kleffner, M. A., Mclaughlin, P. I., Loydell, D. K., Munnecke, A., Jeppsson, L., Corradini, C., Brunton, F. R., and Saltzman, M. R.: Revised correlation of Silurian Provincial Series of North America with global and regional chronostratigraphic units and $d^{13}C_{carb}$ chemostratigraphy, Lethaia, 44, 185–202, https://doi.org/10.1111/j.1502-3931.2010.00234.x, 2010.

Cramer, B. D., Condon, D. J., Söderlund, U., Marshall, C., Worton, G. J., Thomas, A. T., Calner, M., Ray, D. C., Perrier, V., Boomer, I., Patchett, P. J., and Jeppsson, L.: U-Pb (zircon) age constraints on the timing and duration of wenlock (Silurian) paleocommunity collapse and recovery during the "Big Crisis", Bull. Geol. Soc. Am., 124, 1841–1857, https://doi.org/10.1130/B30642.1, 2012.

Cramer, F. H.: Chitinozoans of a composite section of Upper Llandoverian to basal Lower Gedinnian sediments in northern León, Spain, A preliminary report, Bulletin de la Societe Beige de Geologie, de Paleontologie et d'Hydrologie, 75, 69–129, 1967.

da Costa, N. M.: Quitinozoários Silurianos do Igarapé da Rainha, Estado do Pará, Divisão de Geologia e Mineralogia, Departamento Nacional de Produção Minera, Boletim, 255, 1–101, 1971.

Daoust, P.: High resolution stratigraphy of the lower Silurian (Rhuddanian-Aeronian) paleotropical neritic carbonates, Anticosti Island, Québec, Unpublished MSc. Thesis, UOttawa, 2017.

Davies, J. R., Waters, R. A., Molyneux, S. G., Williams, M., Zalasiewicz, J. A., Vandenbroucke, T. R. A., and Verniers, J.: A revised sedimentary and biostratigraphical architecture for the Type Llandovery area, Central Wales, Geol. Mag., 150, 300–332, https://doi.org/10.1017/S0016756812000337, 2013.

De Backer, T., Day, J. E., Emsbo, P., Mclaughlin, P. I., and Vandenbroucke, T. R. A.: Chitinozoan response to the "Kellwasser events": population dynamics and morphological deformities across the Frasnian-Famennian mass extinction, Pap. Palaeontol., 10, e1557, https://doi.org/10.1002/spp2.1557, 2024.

De Decker, S.: An integrated early Silurian biochemostratigraphy of the La Loutre #1 drill core in Anticosti Island, Canada, Unpublished MSc thesis, UGent, 2017.

Delabroye, A., Munnecke, A., Servais, T., Vandenbroucke, T. R. A., and Vecoli, M.: Abnormal forms of acritarchs (phytoplankton) in the upper Hirnantian (Upper Ordovician) of Anticosti Island, Canada, Rev. Palaeobot. Palyno., 173, 46–56, https://doi.org/10.1016/j.revpalbo.2011.10.010, 2012.

Desrochers, A.: Rocky shoreline deposits in the Lower Silurian (upper Llandovery, Telychian) Chicotte Formation, Anticosti Island, Quebec, Can. J. Earth Sci., 43, 1205–1214, https://doi.org/10.1139/E06-054, 2006.

Eisenack, A.: Neue Mikrofossilien des baltischen Silurs 1, Palaeontol. Z., 13, 74–118, 1931.

Eisenack, A.: Neue Mikrofossilien des baltischen Silurs. III. und neue Mikrofossilien des böhmischen Silurs. I, Palaeontol. Z., 16, 52–76, https://doi.org/10.1007/BF03041667, 1934.

Eisenack, A.: Neue Chitinozoen aus dem Silur des Baltikums und dem Devon der Eifel, Senckenbergiana Lethaea, 36, 311–319, 1955.

Eisenack, A.: Neotypen baltischer Silur-Chitinozoen und neue Arten, Neues Jahrb. Geol. P. Abh., 108, 1–20, 1959.

Eisenack, A.: Weitere Mikrofossilien aus dem Beyrichienkalk (Silur), Neues Jahrb. Geol. P. M., 8, 449–460, 1971.

Eisenack, A.: Beitrage zur chitinozoen Forschung, Palaeontographica A, 140, 117–130, 1972.

Emsbo, P.: Sedex brine expulsions to Paleozoic basins may have changed global marine $^{87}Sr/^{86}Sr$ values, triggered anoxia, and initiated mass extinctions, Ore Geol. Rev., 86, 474–486, https://doi.org/10.1016/j.oregeorev.2017.02.031, 2017.

Ghienne, J. F., Desrochers, A., Vandenbroucke, T. R., Achab, A., Asselin, E., Dabard, M. P., Farley, C., Loi, A., Paris, F., Wickson, S., and Veizer, J.: A Cenozoic-style scenario for the end-Ordovician glaciation, Nat. Commun., 5, 4485, https://doi.org/10.1038/ncomms5485, 2014.

Harper, D. A. T., Hammarlund, E. U., and Rasmussen, C. M. Ø.: End Ordovician extinctions: A coincidence of causes, Gondwana Res., 25, 1294–1307, https://doi.org/10.1016/j.gr.2012.12.021, 2014.

Hints, O., Killing, M., Männik, P., and Nestor, V.: Frequency patterns of chitinozoans, scolecodonts, and conodonts in the upper Llandovery and lower Wenlock of the Paatsalu core, western Estonia, P. Est. Acad. Sci., 55, 128–155, https://doi.org/10.3176/geol.2006.2.04, 2006.

Jin, J. and Copper, P.: Canadian Society of Petroleum Geologists, and Geological Association of Canada: Late Ordovician and early Silurian pentamerid brachiopods from Anticosti Island, Québec, Canada, Canadian Society of Petroleum Geologists, 18, 1–140, https://doi.org/10.1017/S0022336000030973, 2000.

Jin, J., Harper, D. A. T., Cocks, L. R. M., McCausland, P. J. A., Rasmussen, C. M. Ø., and Sheehan, P. M.: Precisely locating the Ordovician equator in Laurentia, Geology, 41, 107–110, https://doi.org/10.1130/G33688.1, 2013.

Kaljo, D., Martma, T., Männik, P., and Viira, V.: Implications of Gondwana glaciations in the Baltic late Ordovician and Silurian and a carbon isotopic test of environmental cyclicity, Bull. Soc. Géol. Fr., 174, 59–66, https://doi.org/10.2113/174.1.59, 2003.

Klock, C., Calner, M., McLaughlin, P. I., Emsbo, and Vandenbroucke, T. R. A.: Stratigraphic trends in chitinozoan teratology across the Silurian Mulde Event in the distal Baltic Basin (Gotland, Sweden), in: 68th Palaeontological Association Annual Meeting, 9–13 December 2024, Friedrich-Alexander Universität, Erlangen-Nürnberg, Germany, 2024a.

Klock, C., Desrochers, A., McLaughlin, P. I., Emsbo, P., De Backer, T., Jonckheere, F. M., Esteves, C. J. P., and Vandenbroucke, T. R. A.: Chitinozoan biostratigraphy through the Aeronian–Telychian boundary interval on Anticosti Island, Canada, J. Micropalaeontol., 43, 475–495, https://doi.org/10.5194/jm-43-475-2024, 2024b.

Long, D. G. F.: Tempestite frequency curves: A key to Late Ordovician and Early Silurian subsidence, sea-level change, and orbital forcing in the Anticosti foreland basin, Quebec, Canada, Can. J. Earth Sci., 44, 413–431, https://doi.org/10.1139/E06-099, 2007.

Loydell, D. K., Männik, P., and Nestor, V.: Integrated biostratigraphy of the lower Silurian of the Aizpute-41 core, Latvia, Geol. Mag., 140, 205–229, https://doi.org/10.1017/S0016756802007264, 2003.

Loydell, D. K., Nestor, V., and Männik, P.: Integrated biostratigraphy of the lower silurian of the Kolka-54 core, Latvia, Geol. Mag., 147, 253–280, https://doi.org/10.1017/S0016756809990574, 2010.

Männik, P., Loydell, D. K., Nestor, V., and Nõlvak, J.: Integrated Upper Ordovician–lower Silurian biostratigraphy of the Grötlingbo-1 core section, Sweden, GFF, 137, 226–244, https://doi.org/10.1080/11035897.2015.1042032, 2015.

McAdams, N. E. B., Cramer, B. D., Bancroft, A. M., Melchin, M. J., Devera, J. A., and Day, J. E.: Integrated $\delta^{13}$Ccarb conodont, and graptolite biochemostratigraphy of the Silurian from the Illinois Basin and stratigraphic revision of the Bainbridge Group, Geol. Soc. Am. Bull., 131, 335–352, https://doi.org/10.1130/B32033.1, 2019.

McLaughlin, P. I., Emsbo, P., Brett, C. E., Bancroft, A. M., Desrochers, A., and Vandenbroucke, T. R. A.: The rise of pinnacle reefs: A step change in marine evolution triggered by perturbation of the global carbon cycle, Earth Planet. Sc. Lett., 515, 13–25, https://doi.org/10.1016/j.epsl.2019.02.039, 2019.

Melchin, M. J., Sadler, P. M., and Cramer, B. D.: The Silurian period, in: The Geologic Time Scale 2012, Chap. 22, edited by: Gradstein, F. M., Ogg, J. G., Schmitz, M., and Ogg, G., Elsevier, New York, 525–558, ISBN 978-0-44-459425-9, 2012.

Melchin, M. J., Sadler, P. M., and Cramer, B. D.: The Silurian period, in: Geologic Time Scale 2020, Vol. 2, edited by: Gradstein, F. M., Ogg, J. G., Schmitz, M. D., and Ogg, G. M., Elsevier, Amsterdam, 695–732, https://doi.org/10.1016/C2020-1-02369-3, 2020.

Melchin, M. J., Davies, J. R., Boom, A., De Weirdt, J., McIntyre, A. J., Russel, C., Vandenbrouck, T. R. A., and Zalasiewicz, J. A.: Integrated stratigraphical study of the Rhuddanian-Aeronian (Llandovery, Silurian) boundary succession in the Rheidol Gorge, Wales: a proposed Global Stratotype Section and Point for the base of the Aeronian Stage, Lethaia, 56, 1–23, https://doi.org/10.18261/let.56.1.8C, 2023.

Munnecke, A. and Männik, P.: New biostratigraphic and chemostratigraphic data from the Chicotte Formation (Llandovery, Anticosti Island, Laurentia) compared with the Viki core (Estonia, Baltica), Estonian J. Earth Sci., 58, 159–169, https://doi.org/10.3176/earth.2009.3.01, 2009.

Munnecke, A., Samtleben, C., and Bickert, T.: The Ireviken Event in the lower Silurian of Gotland, Sweden – Relation to similar Palaeozoic and Proterozoic events, Palaeogeogr. Palaeocl., 195, 99–124, https://doi.org/10.1016/S0031-0182(03)00304-3, 2003.

Munnecke, A., Calner, M., Harper, D. A. T., and Servais, T.: Ordovician and Silurian sea-water chemistry, sea level, and climate: A synopsis, Palaeogeogr. Palaeocl., 296, 389–413, https://doi.org/10.1016/j.palaeo.2010.08.001, 2010.

Munnecke, A., Delabroye, A., Servais, T., Vandenbroucke, T. R. A., and Vecoli, M.: Systematic occurrences of malformed (teratological) acritarchs in the run-up of Early Palaeozoic $\delta^{13}$C isotope excursions, Palaeogeogr. Palaeocl., 367–368, 137–146, https://doi.org/10.1016/j.palaeo.2012.02.029, 2012.

Nestor, H. and Nestor, V.: Upper Llandovery to middle Wenlock (Silurian) lithostratigraphy and chitinozoan biostratigraphy in southwestern Estonia and northernmost Latvia, P. Est. Acad. Sci. Geol., 51, 67–87, https://doi.org/10.3176/geol.2002.2.01, 2002.

Nestor, V.: Middle Llandoverian Chitinozoans from Estonia, Proceedings of the Academy of Sciences of the Estonian SSR, Geology, 29, 136, https://doi.org/10.3176/geol.1980.4.03, 1980.

Nestor, V.: New Wenlockian species of Conochitina from Estonia, Eesti NSV Teaduste Akadeemia Toimetised, Geoloogia, 31, 105–111, https://doi.org/10.3176/geol.1982.3.04, 1982.

Nestor, V.: Silurian Chitinozoans, in: Field Meeting Estonia, 1990, An Excursion Guidebook, edited by: Kaljo, D. and Nestor, H., Tallinn: Estonian Academy of Sciences, 1990.

Nestor, V.: Early Silurian chitinozoans of Estonia and North of Latvia, Academia, 4, 1–163, 1994.

Nestor, V.: Chitinozoan biostratigraphy of the Přidoli Series of the East Baltic, Est. J. Earth Sci., 60, 191–206, https://doi.org/10.3176/earth.2011.4.01, 2011.

Nestor, V.: A summary and revision of the East Baltic Silurian chitinozoan biozonation, Est. J. Earth Sci., 61, 242–260, https://doi.org/10.3176/earth.2012.4.05, 2012.

Paris, F.: Les chitinozoaires dans le Paléozoïque du sud-ouest de l'Europe (cadre géologique-étude systématique-biostratigraphie), Bull. Soc. géol. minéral. Bretagne, 26, 1–496, 1981.

Paris, F., Grahn, Y., Nestor, V., and Lakova, I.: A revised chitinozoan classification, J. Paleontol., 73, 549–570, https://doi.org/10.1017/S0022336000032388, 1999.

Rasmussen, C. M. Ø., Vandenbroucke, T. R. A., Nogues-Bravo, D., and Finnegan, S.: Was the Late Ordovician mass extinction truly exceptional, Trends Ecol. Evol., 38, 812–821, https://doi.org/10.1016/j.tree.2023.04.009, 2023.

Riva, J. F. and Petryk, A. A.: Graptolites from the Upper Ordovician and Lower Silurian of Anticosti Island and the Position of the Ordovician-Silurian Boundary, in: Field Meeting Anticosti-Gaspé – Subcommission on Silurian Stratigraphy, Ordovician–Silurian Boundary Working Group, edited by: Lespérance, P. J., Université de Montréal, Québec, 143–157, 1981.

Sami, T. and Desrochers, A.: Episodic sedimentation on an early Silurian, storm-dominated carbonate ramp, Becscie and Merrimack formations, Anticosti Island, Canada, Sedimentology, 39, 355–381, https://doi.org/10.1111/j.1365-3091.1992.tb02122.x, 1992.

Schallreuter, R.: Neue Chitinozoen aus ordovizischen Geschieben und Bemerkungen zur Gattung *Illichitina*, Palaeontologische Abhandlungen, 1, 392–405, 1963.

Schindelin, J., Arganda-Carreras, I., Frise, E., Kaynig, V., Longair, M., Pietzsch, T., Preibisch, S., Rueden, C., Saalfeld, S., Schmid, B., Tinevez, J.-Y., White, D. J., Hartenstein, V., Eliceiri, K., Tomancak, P., and Cardona, A.: Fiji: an open-source platform for biological-image analysis, Nat. Methods, 9, 676–682, https://doi.org/10.1038/nmeth.2019, 2012.

Soufiane, A. and Achab, A.: Chitinozoan zonation of the Late Ordovician and the Early Silurian of the island of Anticosti, Québec, Canada, Rev. Palaeobot. Palyno., 109, 85–111, https://doi.org/10.1016/S0034-6667(99)00044-5, 2000.

Sutherland, S. J. E.: Ludlow chitinozoans from the type area and adjacent regions, Palaeontogr. Soc. Monogr., 148, 1–104, https://doi.org/10.1080/25761900.2022.12131775, 1994.

Taugourdeau, P.: Etude de quelques espèces critiques de Chitinozoaires de la region d'Edjelé et compléments à la faune locale, Rev. Micropal, 6, 130–144, 1963.

Taugourdeau, P.: Les Chitinozoaires, techniques d'études, morphologie et classification, Mémoire de la Société Géologique de France, Nouvelle Série, 45, 1–64, 1966.

Umnova, N. I.: Structural types of the prosome and operculum in the association with genera and species of chitinozoans, Paleontol. J., 4, 393–405, 1976.

Vancoppenolle, I., Emsbo, P., McLaughlin, P. I., Calner, M., and Vandenbroucke, T. R. A.: A surge of malformed chitinozoans accompanies the onset of the Ireviken Event, in: 68th Palaeontological Association Annual Meeting, 9–13 December 2024, Friedrich-Alexander Universität, Erlanden-Nürnberg, Germany, 2024.

Vandenbroucke, T. R. A., Verniers, J., and Clarkson, E. N. K.: A chitinozoan biostratigraphy of the Upper Ordovician and lower Silurian strata of the Girvan area, Midland Valley, Scotland, Earth Env. Sci. T. R. Soc., 93, 111–134, https://doi.org/10.1017/S0263593300000365, 2003.

Vandenbroucke, T. R. A., Emsbo, P., Munnecke, A., Nuns, N., Duponchel, L., Lepot, K., Quijada, M., Paris, F., Servais, T., and Kiessling, W.: Metal-induced malformations in early Palaeozoic plankton are harbingers of mass extinction, Nat. Commun., 6, 7966, https://doi.org/10.1038/ncomms8966, 2015.

van de Schootbrugge, B., Tremolada, F., Rosenthal, Y., Bailey, T. R., Feist-Burkhardt, S., Brinkhuis, H., Pross, J., Kent, D. V., and Falkowski, P. G.: End-Triassic calcification crisis and blooms of organic-walled "disaster species", Palaeogeogr. Palaeocl., 244, 126–141, https://doi.org/10.1016/j.palaeo.2006.06.026, 2007.

Verniers, J., Nestor, V., Paris, F., Dufka, P., Sutherland, S., and Van Grootel, G.: A global Chitinozoa biozonation for the Silurian, Geol. Mag., 132, 651–666, https://doi.org/10.1017/S0016756800018896, 1995.

Wilson, L. R. and Hedlund, R. W.: Calpichitina scabiosa, a new Chitinozoan from the Sylvan Shale (Ordovician) of Oklahoma, Oklahoma Geological Notes, 24, 161–164, 1964.

Zhang, S. and Barnes, C. R.: A New Llandovery (Early Silurian) Conodont Biozonation and Conodonts from the Becscie, Merrimack, and Gun River Formations, Anticosti Island, Québec, J. Paleontol., 57, 1–46, 2002.